Ore Geology Reviews 123 (2020) 103574

Contents lists available at ScienceDirect

Ore Geology Reviews

journal homepage: www.elsevier.com/locate/oregeorev

Flat-slab subduction and formation of "intraplate" porphyry deposits: Insights from the Jurassic high and low La/Yb ore-forming porphyries along the Qin-Hang belt, South China

Long Ren[a], Zhiwei Bao[a], Wenting Huang[a], Shuping Lin[b], Shixiong Xie[a,c], Juan Liao[a,c], Jing Li[d], Huaying Liang[a,*]

[a] Key Laboratory of Mineralogy and Metallogeny, Guangzhou Institute of Geochemistry, Chinese Academy of Sciences, Guangzhou 510640, China
[b] Chongqing Key Laboratory of Geological Survey of Land Quality, Chongqing 404100, China
[c] University of Chinese Academy of Sciences, Beijing 100049, China
[d] Zijin Mining Group Co, Ltd, Shanghang 364200, China

ARTICLE INFO

Keywords:
"Intraplate" porphyry deposit
Petrogenesis
Metallogeny
Flat-slab subduction
South China Block

ABSTRACT

The Middle-Late Jurassic porphyry deposits with different element associations in the interior of South China Block are over 1000 km away from subduction zone, which conflicts with the traditional belief that the porphyry Cu-Au-Mo deposits were formed in the convergent margin. However, their genesis and geodynamics are still under debate. To address the above issues, this paper reports new geochronological, mineralogical, elemental and isotopic data for the Yuanzhuding porphyry deposit from Qin-Hang belt, and compared with the published data of porphyry deposits in this belt. The Yuanzhuding porphyry deposit has zircon U-Pb and molybdenite Re-Os ages of 154.6–155.2 Ma and 156.3 Ma respectively, which suggest that it is contemporaneous with the Middle-Late Jurassic Dexing, Baoshan and Dabaoshan porphyry deposits in the belt. The Yuanzhuding and Dexing porphyries have adakitic signatures and Nd-Hf isotopes similar to the contemporaneous EMI-type-mantle-derived mafic rocks featuring high Nb, P_2O_5 and LILEs/HFSEs values, suggestive of their roots in EMI-type lithospheric mantle hybridized by basaltic-slab-derived melts and pelagic-sediments-derived fluids. Combined with the slightly lower Nd isotopes of Yuanzhuding porphyry than Dexing porphyry, the fractionation modeling suggests that they were formed via AFC and FC processes of basaltic magma respectively and that their adakitic signatures can be attributed to hornblende fractionation. In contrast, the Baoshan and Dabaoshan porphyries have high Yb contents, low $(La/Yb)_N$ ratios and Nd-Hf isotopes similar to the Proterozoic crust in the region. Mineral and whole-rock elemental plots reveal that they were stemmed from FC processes of partial melts of the Proterozoic crust, with involvement of voluminous and a little EMI-type-mantle-derived basaltic magma respectively. Integrated with the spatio-temporal evolution of Triassic-Jurassic magmatic, metamorphic, sedimentary, tectonic and structural records in the region, the petrogenesis of ore-forming porphyries indicates that the porphyry deposits were controlled by the northwestward flat-slab subduction and related slab break-off. The basaltic magma sourced from the EMI-type mantle had high Cu, H_2O and S contents and oxidized signature, which are favorable for the formation of Dexing porphyry Cu-Au-Mo mineralization via differentiation and volatile exsolution in a closed magma chamber. Also, it can incorporate crustal materials via AFC processes, thus forming Yuanzhuding porphyry Cu-Mo mineralization. In addition, the thick crust caused by flat-slab subduction facilitated the input of voluminous and a little basaltic magma into crustal Baoshan and Dabaoshan porphyries, thus generating Pb-Zn-Cu-Mo and Mo-W-Pb-Zn mineralization, respectively. We, therefore, propose that the "intraplate" porphyry deposits with different element associations result from complicated crust-mantle interaction in the thick "intraplate" crust, and that their metallogenic elements will change from Cu-Au-Mo- to Mo-W-Pb-Zn-dominated mineralization with the transformation of magma sources from enriched-mantle- to continental-crust-dominated materials.

* Corresponding author at: Key Laboratory of Mineralogy and Metallogeny, Guangzhou Institute of Geochemistry, Chinese Academy of Sciences, Guangzhou 510640, China.
E-mail address: lianghy@gig.ac.cn (H. Liang).

https://doi.org/10.1016/j.oregeorev.2020.103574
Received 16 January 2020; Received in revised form 18 April 2020; Accepted 4 May 2020
Available online 07 May 2020
0169-1368/

1. Introduction

As the porphyry deposits host the most important resources of Cu, Mo and Au in the world, they have long been a research hotspot in the field of economic geology (Silitoe, 2010; Liang et al., 2018). They are commonly related to the oxidized magma and were mainly formed in the convergent margins including continental margin arc and collisional orogen (Camus and Dilles, 2001; Liang et al., 2006, 2009; Richards, 2009; Sun et al., 2013; Hou et al., 2009, 2015; Zou et al., 2017; Huang et al., 2019, 2020). Porphyry deposits above the slab subduction setting are closely related to calc-alkaline felsic magma, which can be traced back to basaltic partial melts of mantle wedge incorporating fluids released by slab dehydration or direct slab-melts, whilst those in collisional orogen feature high-K calc-alkaline and shoshonitic magma generated via the partial melting of thickened juvenile lower crust (Richards, 2003; Liang et al., 2006, 2009; Hou et al., 2009; Richards, 2009; Sun et al., 2015; Chen et al., 2016). The South China Block, hosting the most abundant Mesozoic poly-metallic mineral resources in China, contains a series of Middle–Late Jurassic porphyry Cu-Au-Mo-W-Pb-Zn deposits in its interior, which are over 1000 km away from the subduction zone and were commonly thought to be formed in the intraplate setting (Zhong et al., 2016; Huang et al., 2017). This is in contradiction to the traditional belief that the porphyry Cu-Au-Mo deposits were formed in the convergent margin (Zhang et al., 2013). Although numerous investigations have been carried out, the genesis and geodynamic models of these “intraplate” porphyry deposits are still under debate, with the proposed models including the partial melting of a thickened juvenile lower crust in an intraplate setting, partial melting of delaminated lower crust, slab melting related to ridge subduction and oblique subduction (Wang et al., 2006; Sun et al., 2010; Hou et al., 2013; Mao et al., 2013; Zhang et al., 2013).

The paleomagnetic, sedimentary, metamorphic magmatic records in the region have confirmed that the South China Block has been a single and coherent terrane since the Neoproterozoic continental collision between Yangtze and Cathaysia Blocks along a lithospheric suture zone that is close to the Qin-Hang (or Shi-Hang) zone (Goodell et al., 1991; Li et al., 2002; Zhou et al., 2002). The Middle–Late Jurassic “intrplate” porphyry Cu-Au-Mo-W-Pb-Zn deposits in the South China Block are distributed along the Qin-Hang belt, which mainly contain Yuanzhuding, Dabaoshan, Baoshan and Dexing deposits from south to north, thus forming a giant porphyry metallogenic belt (Fig. 1; Xie et al., 2013; Zhong et al., 2013; Wang et al., 2015; Li et al., 2018a; Mi et al., 2018). Despite similar formation ages (170–156 Ma; Mao et al., 2013), they display different ore-forming element associations: 1) the Yuanzhuding porphyry deposit characterized by Cu-Mo-dominated mineralization (Zhong et al., 2013); 2) the Dexing deposit featuring Cu-dominated Cu-Au-Mo mineralization (Hou et al., 2013; Wang et al., 2015); 3) the Baoshan deposit featuring Pb-Zn-dominated Pb-Zn-Cu-Mo mineralization (Li et al., 2019a); 4) the Dabaoshan deposit featured by Mo-W-dominated Mo-W-Pb-Zn mineralization (Wang et al., 2011). However, there is no consensus on what factors yielded these porphyry deposits with different element associations. For example, given that the low Cl fugacity can limit the efficiency of Cu extraction and transportation, Mao et al. (2018) attributed the fact that the Yuanzhuding deposit hosts similar Mo reserves but much less Cu reserves compared to the Dexing deposit to the much lower Cl fugacity in ore-forming fluid in Yuanzhuding than Dexing deposits. The low Cu concentrations of fresh samples of the Yuanzhuding porphyry are inconsistent with this inference.

In this contribution, we present new zircon U-Pb ages, trace elements and in-situ Hf isotopes, molybdenite Re-Os ages, whole-rock major and trace elements and whole-rock Sr and Nd isotopic compositions for the Yuanzhuding porphyry deposit from Qin-Hang belt in the interior of South China Block, and compared with the published data of porphyry deposits in this belt, with the aim of: (1) illuminating the genesis and geodynamic model of “intraplate” porphyry deposits; (2) shedding light on the critical factors controlling the formation of porphyry deposits with different element associations.

2. Geological setting

2.1. Regional geology

The South China Block was formed by the Neoproterozoic continental collision (ca. 870–860 Ma) between the Yangtze Block in northwest and the Cathaysia Block in southeast along a tectonic suture zone, namely Jiangshan–Shaoxing fault zone (Fig. 1; Chen and Jahn, 1998). From then on, the Yangtze and Cathaysia Blocks have been consolidated into a single and coherent terrane and entered an intraplate evolution stage (Wang et al., 2006). The Yangtze Block has an Archean crystalline basement mainly composed of TTG gneisses and amphibolites, which was overlain by the Late Mesoproterozoic to Early Neoproterozoic metavolcanic-sedimentary successions (Zhang et al., 2002; Zhao and Cawood, 2012). The Cathaysia Block has a Proterozoic crystalline basement (Zhao et al., 2014). The Neoproterozoic convergence of Yangtze and Cathaysia Blocks produced the Shuangxiwu Group (ca. 970–890 Ma), which mainly contains metamorphosed arc volcanic rocks and metasediments (Li et al., 2009). Then, the South China Block experienced the Neoproterozoic to Triassic sedimentation and Early Paleozoic intra-continental orogeny until it collided with the Indochina Block and North China Craton in the Triassic (Carter et al., 2001; Ernst et al., 2007; Charvet, 2013).

The South China Block hosts the most abundant poly-metallic mineral resources in China, especially W, Sn, Bi, Cu, Ag, Sb, Hg, rare metals and heavy rare earth elements mainly formed in the Mesozoic (Mao et al., 2004). Three Mesozoic magmatic and metallogenic events with distinct metal and rock association and spatial-temporal distribution were recognized in the South China Block (Mao et al., 2013), which include the Late Triassic (230–210 Ma), Middle–Late Jurassic (170–150 Ma) and Early–Middle Cretaceous (120–80 Ma) flare-ups. The Middle–Late Jurassic magmatic and metallogenic event mainly concerns the porphyry–skarn Cu-Au-Mo-W-Pb-Zn deposits with ages of ca. 156–170 Ma and granite-related polymetallic W–Sn deposits with ages of ca. 150–160 Ma (Fig. 1; Mao et al., 2013). Intriguingly, the Middle–Late Jurassic porphyry Cu-Au-Mo-W-Pb-Zn deposits, including Dexing, Baoshan, Dabaoshan and Yuanzhuding deposits, are distributed along the Qin-Hang zone from north to south (Fig. 1).

2.2. Deposit geology and intrusion petrology

Located at the southwest of the Qin-Hang porphyry metallogenic belt, the Yuanzhuding porphyry Cu-Mo deposit has reserve of 0.98 Mt Cu at grades of 0.17%, 0.26 Mt Mo at grades of 0.045% and 478 t Ag at grades of 0.43 g/t (Chu, 2013; Mao et al., 2018). The Yuanzhuding granite porphyry with an outcrop area of 0.20 km^2 intrudes the Cambrian clastic sedimentary rocks along the anticline axis (Fig. 2; Chu et al., 2013; Zhong et al., 2013) and exhibits a typical porphyritic structure (Fig. 3A, B). Phenocrysts are mainly quartz, K-feldspar, plagioclase, and minor biotite. The matrix has a microcrystalline texture and comprises mainly plagioclase, K-feldspar, quartz and biotite microlites. The accessory minerals include zircon, apatite and pyrite. The strong alternation that the granite porphyry underwent can be divided into (Fig. 3C and D): potassic alternation in the early stage (Fig. 3C); silicon alternation in the second stage (Fig. 3C); muscovite-sulfide veinlet in the third stage (Fig. 3D); and low-temperature alternation featured by carbonatization, chloritization and epidotization in the fourth stage. The ore minerals include molybdenite, pyrite, chalcopyrite and minor bornite, while the gangue minerals include quartz, feldspar, biotite and sericite.

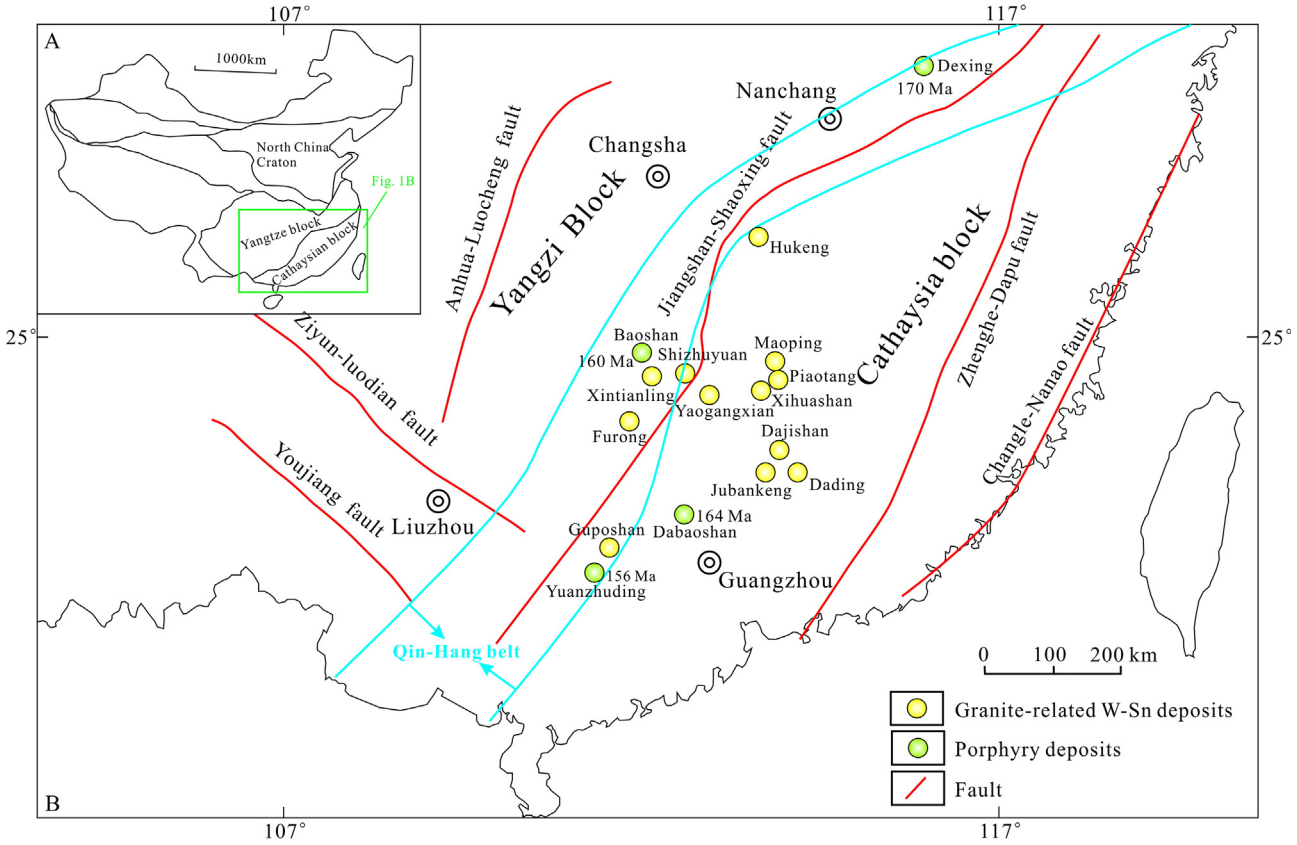

Fig. 1. (A) Inset shows location of the South China Block in China. (B) Tectonic framework of South China Block shows distribution of main tectonic blocks, faults and the Middle–Late Jurassic porphyry and granite-related W-Sn deposits (modified from Mao et al., 2013). Ages of porphyry deposits are from this study, Wang et al. (2011, 2015) and Lu et al. (2006).

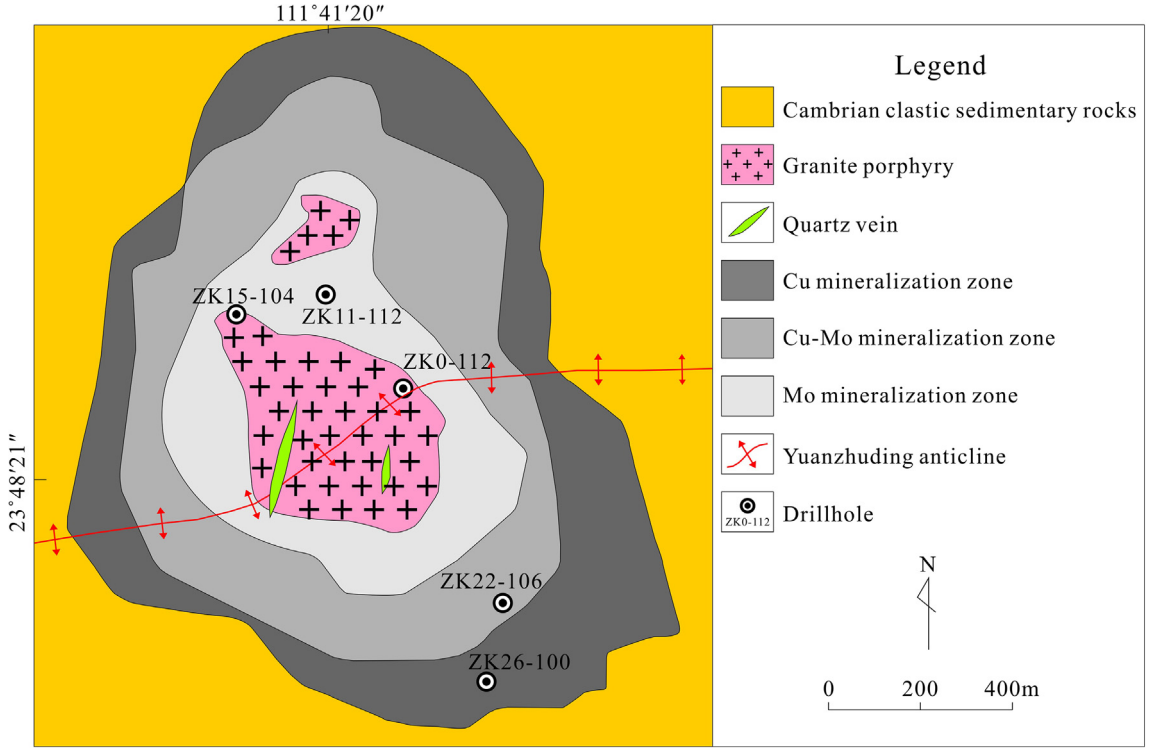

Fig. 2. Simplified geological map of Yuanzhuding deposit showing the distribution of Cu–Mo mineralization and granite porphyry (revised from Zhong et al., 2013).

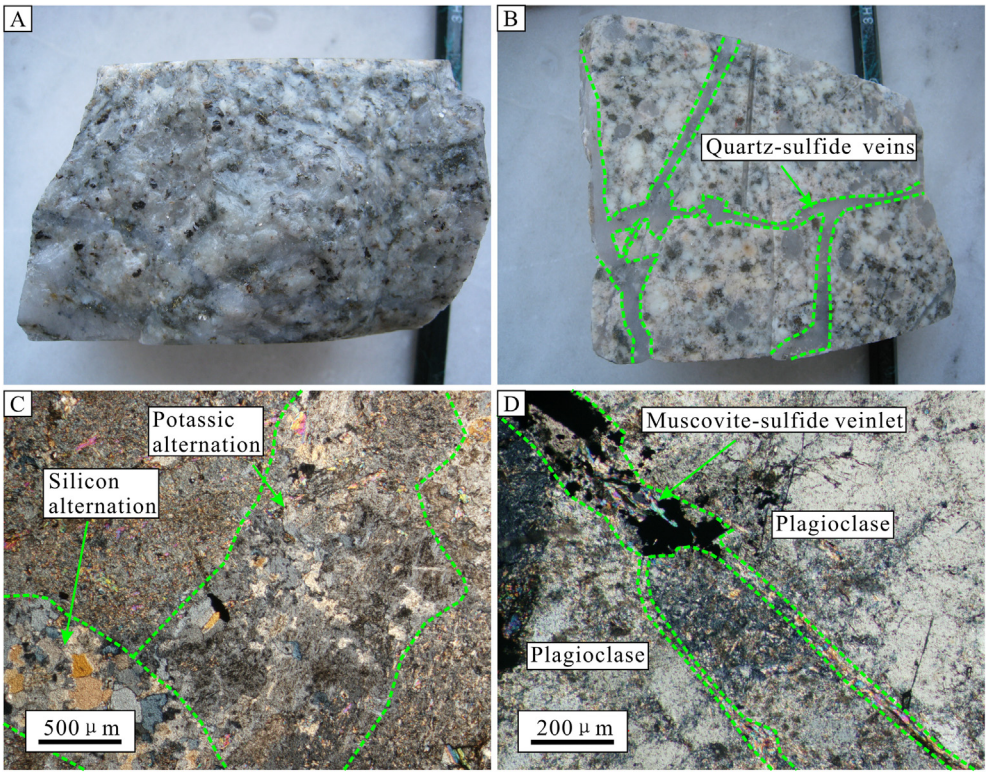

Fig. 3. Representative field occurrence and thin section petrography of the Yuanzhuding porphyry: (A) specimen of the Yuanzhuding porphyry; (B) porphyry developed typical porphyritic texture and quartz-sulfide veins; (C) the early potassic alternation is intersected by later silicon alteration; (D) the plagioclase in porphyry is intersected by muscovite-sulfide veinlet.

3. Analytical methods

3.1. Zircon U-Pb dating and elemental and Hf isotopic analyses

Zircon crystals from the Yuanzhuding porphyry were handpicked via a binocular microscope. The large zircons were preferentially mounted in epoxy and polished. Their cathodoluminescence (CL) imaging, U-Pb dating and elemental analyses were carried out via LA–ICPMS at the Guangzhou Institute of Geochemistry, Chinese Academy of Sciences (GIGCAS). The external calibration standards including NIST standard reference material 610 (NIST610) and standard zircon 91,500 were used for the calculation of U-Pb ages and elemental concentrations. The cumulative probability plots and software ISOPLOT were used to reject inherited zircon and zircon experiencing Pb-loss and yield concordia diagrams respectively (Ludwig, 2003; Liang et al., 2007; Ren et al., 2019). The $^{206}Pb/^{238}U$ age of zircons representing major group was regarded as crystallization age of porphyry.

The coupled MC–ICP-MS and laser ablation system were used for the *in-situ* zircon Lu-Hf isotopic analyses at the GIGCAS. In the course of Lu-Hf isotopic experiment, helium was selected as the carrier gas and laser parameters were featured by beam diameter of 45 μm, repetition rate of 6 Hz and energy density of ~4 J cm^{-2}. The detailed instrument operation and data treatment were reported by Zhang et al. (2014, 2015). This experiment selected zircon Penglai as reference standard and yielded a weighted mean of $^{176}Hf/^{177}Hf$ ratio of 0.282903 ± 0.000015 (2SD; n = 22), which is in accord with the recommended value of Li et al. (2010) within experimental errors.

3.2. Molybdenite Re-Os dating

The molybdenite samples from the Yuanzhuding deposit were smashed to 200 meshes and handpicked via a binocular microscope. The obtained molybdenum grains have a purity of 99% and weight of > 30 mg. Re and Os concentrations and isotopic compositions of molybdenite were tested via a Thermo Electron TJA X–series ICP–MS at the Institute of Geochemistry, Chinese Academy of Sciences. The detailed procedures have been reported by Du et al. (2009).The standard reference material GBW04436 (JDC) was used to test analytical reliability. The total analytical blanks were 1.3 pg for Re and 0.024 pg for common Os. The equation calculating Re–Os model ages is expressed as:

$$t = [\ln(1 + {}^{187}Os/{}^{187}Re)]/\lambda$$

where λ is the decay constant of ^{187}Re at 1.666×10^{-11} $year^{-1}$ (Smoliar et al., 1996). The Re–Os isochron age was obtained via software ISOPLOT (Ludwig, 2003).

3.3. Whole-rock major and trace element analyses

The rock samples crushed to ~ 200-mesh were used for the analyses of major and trace elements. Major and trace elements were analyzed via Rigaku RIX 2000 XRF and Bruker M90 ICP–MS at the GIGCAS respectively. The detailed test procedures have been reported by Li et al., 2004a, 2006. Uncertainties for analyzing major elements are approximately ± 1–2%, whilst accuracies for analyzing trace elements were generally better than ± 5–10%.

3.4. Whole-rock Sr and Nd isotope analyses

The powders of representative rock samples (~80 mg) were firstly used for the chemical treatment at the GIGCAS. The analyses of whole-rock Sr and Nd isotopes were finished via a MC–ICPMS instrument at the GIGCAS. The detailed procedures of chemical treatment and analytical test have been presented by Li et al. (2006). The conventional ion exchange columns and HDEHP-coated Kef columns were used for the separation Sr and Nd respectively. The $^{146}Nd/^{144}Nd$ ratios of 0.7219 and $^{86}Sr/^{88}Sr$ ratios of 0.1194 were used for the correction of mass fractionation of the obtained $^{143}Nd/^{144}Nd$ and $^{86}Sr/^{88}Sr$ ratios respectively. Repeated tests of BHVO-2 and JG-2 standards yielded $^{87}Sr/^{86}Sr$ = 0.703472 ± 0.000023 (2σ, n = 13) and $^{143}Nd/^{144}Nd$ = 0.512217 ± 0.000011 (2σ, n = 13) respectively.

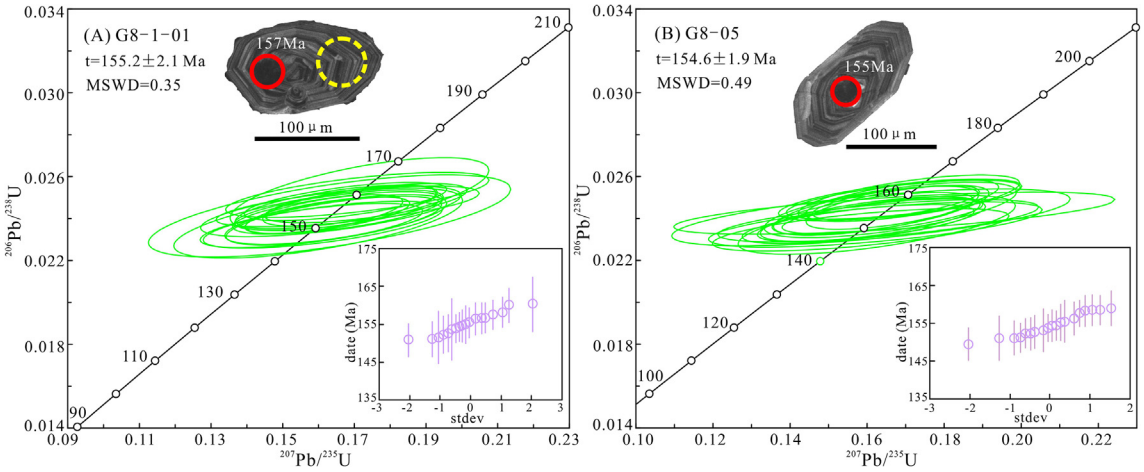

Fig. 4. Zircon U-Pb concordia diagrams and cathodoluminescence images for zircons from the Yuanzhuding porphyry. Insets show cumulative probability diagrams. The red solid and yellow dotted circles represent spots for in-situ U–Pb age and Lu–Hf isotope analyses, with beam diameter of 30 μm and 45 μm, respectively. (For interpretation of the references to colour in this figure legend, the reader is referred to the web version of this article.)

4. Results

4.1. Zircon U-Pb and molybdenite Re-Os ages

Zircon crystals from the Yuanzhuding porphyry are euhedral and prismatic, with 100–200 μm long and 50–100 μm wide. They have typical oscillatory zoning (Fig. 4A and B) and high Th/U ratios (0.40–1.94; Supplementary Table 1), suggestive of a magmatic origin. 24 zircon crystals from sample G8-1-01 were analyzed, of which four discordant results, one older grain (437 Ma) representing inherited/xenocrystic zircon, and one younger grain (132 Ma) suffering Pb-loss were rejected, the remaining 18 LA-ICP-MS tests gave a weighted mean $^{206}Pb/^{238}U$ age of 155.2 ± 2.1 Ma (MSWD = 0.35; Fig. 4A). 25 analyses for zircon from sample G8-05 were determined, of which two discordant results were rejected. Besides, three older (264–711 Ma) and one younger tests (137 Ma), representing inherited/xenocrystic zircon and zircon underwent Pb-loss respectively, were also excluded. The remaining 19 tests yielded a weighted mean $^{206}Pb/^{238}U$ age of 154.6 ± 1.9 Ma (MSWD = 0.49; Fig. 4B). It is concluded that the Yuanzhuding porphyry was formed at ca. 155 Ma.

Molybdenites from the Yuanzhuding porphyry deposit have variable total Re concentrations ranging from 2.69 ppm to 449 ppm and relatively homogeneous model ages ranging from 149.8 Ma to 162.9 Ma (Supplementary Table 2; Zhong et al., 2010; Chen et al., 2012). On the plot of ^{187}Os versus ^{187}Re, they gave an optimum isochron age of 156.3 ± 0.8 Ma (MSWD = 0.75; Fig. 5).

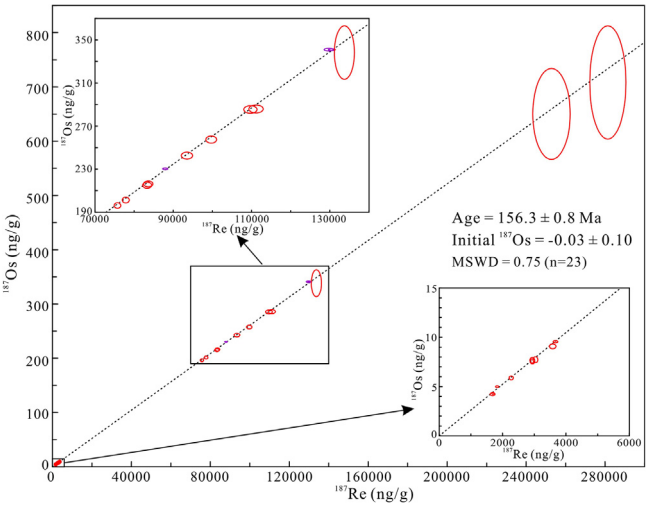

Fig. 5. Molybdenite Re-Os isochrone diagram for the Yuanzhuding porphyry Cu-Mo deposit. Decay constant: $\lambda(^{187}Re) = 1.666 \times 10^{-11}$ year^{-1} (Smoliar et al., 1996), uncertainties are absolute at 2σ. Purple circles represent our new Re-Os isotopic data and red circles represent published data (Zhong et al., 2010; Chen et al., 2012). (For interpretation of the references to colour in this figure legend, the reader is referred to the web version of this article.)

4.2. Zircon trace elements

Given that the zircon LA-ICP-MS trace element analyses might be influenced by small mineral inclusions, we excluded analyses with La > 1 ppm and Ti > 50 ppm that likely reflect the contamination of apatites and Ti-(Fe) oxides. Besides, the following three categories were also eliminated: 1) inherited/xenocrystic zircons; 2) zircons with < 90% concordance; 3) zircon crystals undergoing Pb-loss. The new (Supplementary Table 3) and published zircon trace element compositions of the Yuanzhuding, Dexing, Baoshan and Dabaoshan porphyries (Li et al., 2012; Zhong et al., 2013; Zhang et al., 2017; Mi et al., 2018) were shown in the chondrite-normalized REE patterns and plots of Ce^{4+}/Ce^{3+} versus Eu_N/Eu_N^* (Fig. 6). Zircon crystals from four porphyries display similar REE patterns, with 'magmatic-like' plots, positive Ce anomaly and steep increase from La to Lu (Fig. 6A–C). However, their Eu/Eu* and Ce^{4+}/Ce^{3+} ratios reflecting oxygen fugacity have substantial discrepancy. Zircons from the Yuanzhuding, Dexing and Baoshan porphyries have high Eu/Eu* and Ce^{4+}/Ce^{3+} ratios and significantly positive Ce anomaly, and plot in the field of ore-forming intrusions from northern Chile, while those from the Dabaoshan porphyry exhibit bimodal distribution of Eu/Eu* and Ce^{4+}/Ce^{3+} ratios and moderately positive Ce anomaly, and straddle both the ore-forming and barren intrusions (Fig. 6A–D).

4.3. Whole-rock major and trace elements

4.3.1. Element mobility

Petrographic study indicates that the Yuanzhuding porphyry experienced strong hydrothermal alteration, with varying degrees of silicification, sericitization, chloritization, carbonatization and potassic alteration, and has high contents of loss on ignition (LOI = 2.75 to 7.59 wt%; Supplementary Table 4). Studies have shown that there will be a linear trend between the elements and LOI values if the chemical components of samples were changed by hydrothermal alteration (Wang et al., 2006, 2012). As shown in the plots of elements vs. LOI values (Fig. 7), the major elements including Fe_2O_3, MgO, CaO and

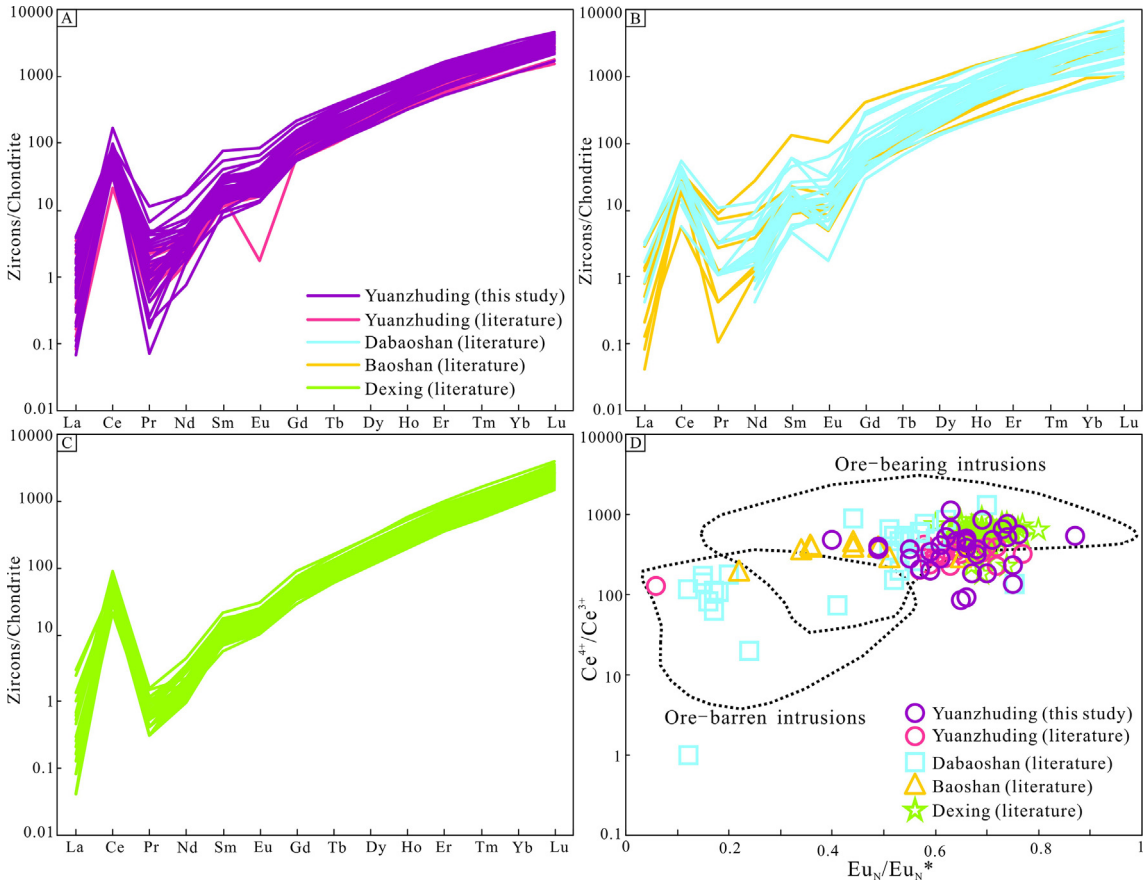

Fig. 6. Zircon trace element plots for the Yuanzhuding, Dexing, Baoshan and Dabaoshan poyphyries: (A-C) chondrite-normalized REE patterns (Sun and McDonough, 1989); (D) Eu_N/Eu_N^* vs. Ce^{4+}/Ce^{3+} plot (the ranges of ore-bearing and barren intrusions from northern Chile are from Ballard et al., 2002; Chen et al., 2019). Data are from this study, Li et al. (2012), Zhong et al. (2013), Zhang et al. (2017) and Mi et al. (2018).

Na_2O and large ion lithophile elements such as Sr and Ba exhibit linear trend, which demonstrate that they are mobile during hydrothermal alteration. In contrast, the TiO_2, Al_2O_3, P_2O_5, transition elements (Co, V, Cr, Ni and Sc), high field-strength elements (Zr, Hf, Nb and Ta), rare-earth elements (REEs), Th and U remain constant, suggestive of their immobility. Therefore, the immobile major element contents (TiO_2, Al_2O_3, P_2O_5) normalized to total 100% anhydrous values, transition elements, high field-strength elements, rare-earth elements, Th and U were used in the following discussion (Supplementary Table 4).

4.3.2. Major and trace elements

Our new (Supplementary Table 4) and published (Liu et al., 2012; Hou et al., 2013; Xie et al., 2013; Zhong et al., 2013; Wang et al., 2015; Huang et al., 2017) whole-rock major and trace elements of the Yuanzhuding, Dexing, Baoshan and Dabaoshan porphyries were used in the following discussion.

The Yuanzhuding granite porphyry has high SiO_2 (71.34–78.16 wt %) and low TiO_2 (0.24–0.36 wt%) and P_2O_5 (0.11–0.15 wt%) contents, plotting in the field of rhyodacite-dacite to rytolite (Fig. 8A). It is characterized by high La (27.4–38.4 ppm) and low Y (6.45–9.22 ppm) and Yb (0.63–0.91 ppm) abundances, generating high $(La/Yb)_N$ ratios of 25.1–37.0 and plotting in the adakite field (Fig. 8B). In the multi-element plots (Fig. 8C and E), it features enrichment in light rare earth elements (LREEs) and large-ion lithophile elements (LILEs; e.g., Cs, Rb, Ba), depletion in heavy rare earth elements (HREEs) and high-field-strength elements (HFSEs; e.g., Nb, Ta, and Ti), fractionated REE patterns, and negligible Eu anomaly (Eu/Eu* = 0.74–0.92).

The Dexing, Baoshan and Dabaoshan porphyries plot in the field of rhyodacite-dacite to rhyolite (Fig. 8A). However, they also show many elemental differences. The Dexing porphyry is featured by low Yb (0.62–1.56 ppm) contents, fractionated REE patterns ($(La/Yb)_N$ = 12.5–35.4) and negligible Eu anomaly (Eu/Eu* = 0.81–1.42; most < 1.10), and plots in the adakite field, which are similar to the Yuanzhuding porphyry. On the contrary, the Baoshan and Dabaoshan porphyries are featured by high Yb (0.89–2.94 ppm) contents, less-fractionated REE patterns ($(La/Yb)_N$ = 6.61–30.6) and mildly negative Eu anomaly (Eu/Eu* = 0.57–1.05; most < 0.8), and plot in the field of calc-alkaline arcs (Fig. 8B–F).

4.4. Radiogenic isotopes

Our new (Supplementary Tables 5 and 6) and published (Liu et al., 2012; Hou et al., 2013; Xie et al., 2013; Zhong et al., 2013; Wang et al., 2015; Huang et al., 2017) whole-rock Sr–Nd and zircon *in-situ* Hf radiogenic isotopes of the Yuanzhuding, Dexing, Baoshan and Dabaoshan porphyries were presented in this section.

Sr isotopes have likely been changed during the hydrothermal alteration, thus being excluded. The Yuanzhuding porphyry has slightly lower Nd and Hf isotopes ($\varepsilon_{Nd}(t)$ = −3.58 to −2.02, and $\varepsilon_{Hf}(t)$ = 0.86–6.32) than the Dexing porphyry ($\varepsilon_{Nd}(t)$ = −1.90–0.60, and $\varepsilon_{Hf}(t)$ = 1.14–7.08). However, the radiogenic isotopes of the Baoshan and Dabaoshan porphyries are distinct from those of the Yuanzhuding and Dexing porphyries. The Baoshan and Dabaoshan porphyries present greatly enriched Nd and Hf isotopes, with $\varepsilon_{Nd}(t)$ and $\varepsilon_{Hf}(t)$ values ranging from −8.20 to −5.00 and from −14.0 to −7.50 respectively, and have two-stage Nd model ages of 1.69–2.09 Ga.

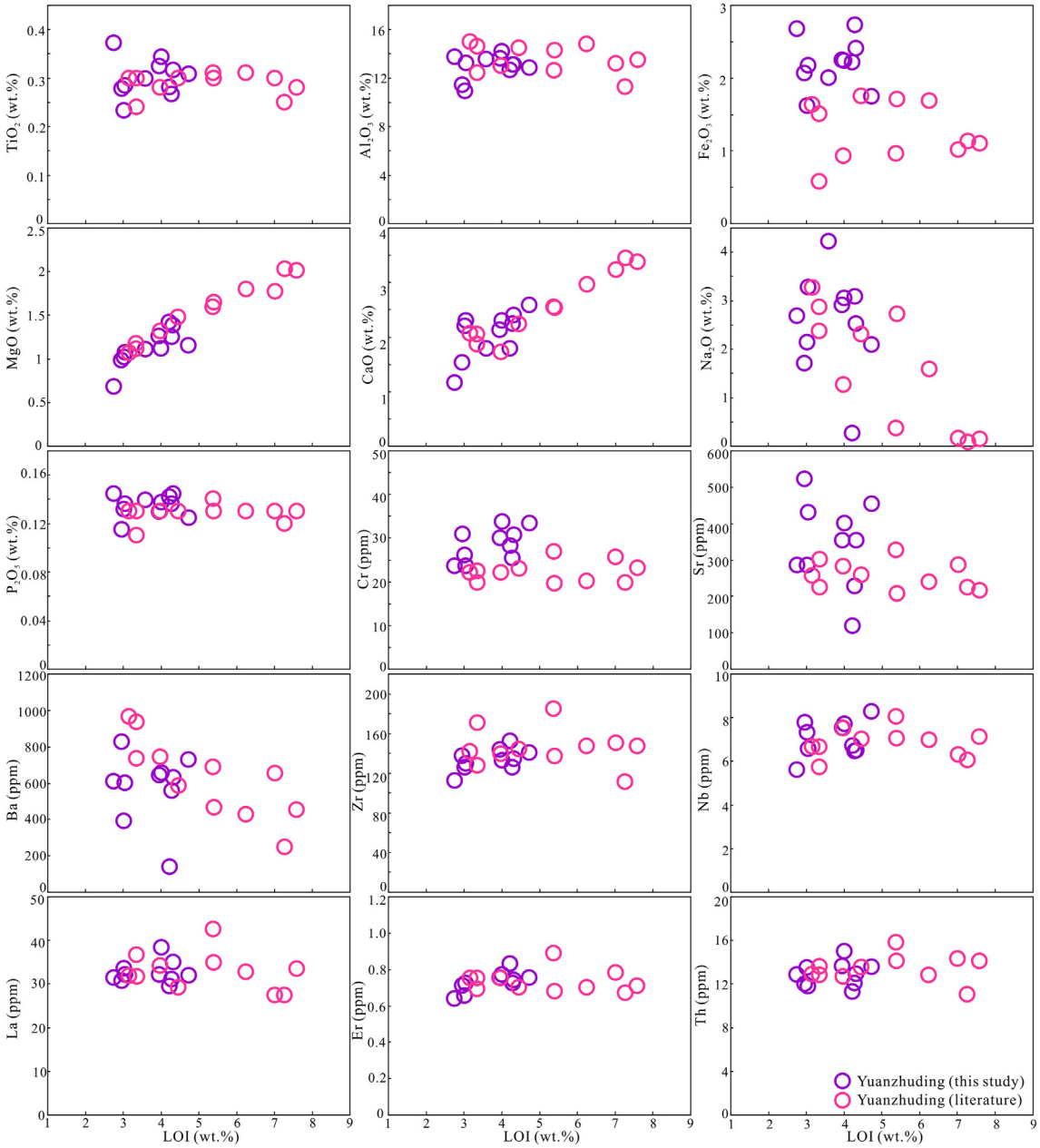

Fig. 7. Plots of elements vs. LOI (wt%) for the Yuanzhuding porphyry.

5. Discussion

5.1. Age of magmatism and related mineralization

The Cu-Mo ore bodies in the Yuanzhuding porphyry deposit are mainly distributed in the *meta*-sandstones around porphyry, indicative of a close spatial relationship between the porphyry and mineralization. Zircons from two porphyry samples yielded a weighted mean $^{206}Pb/^{238}U$ ages of 154.6–155.2 Ma, which are consistent with the molybdenite Re-Os age of 156.3 Ma within a reasonable error range. The close spatio-temporal relationship between the Yuanzhuding porphyry and Cu-Mo mineralization clearly demonstrates their causality. Besides, the zircon U-Pb ages and molybdenite Re-Os age also demonstrate that the Yuanzhuding porphyry Cu-Mo deposit was formed in the Late Jurassic (ca. 155–156 Ma), which is coeval with the Middle-Late Jurassic Dexing, Baoshan and Dabaoshan porphyry deposits in the Qin-Hang belt (Fig. 1; Lu et al., 2006; Wang et al., 2011, 2015).

5.2. Petrogenesis of high La/Yb Yuanzhuding and Dexing porphyries

5.2.1. Adakitic feature

Adakites were originally proposed to define a group of intermediate-felsic volcanic and intrusive rocks featuring high Na_2O (> 3.5 wt%) and Sr (> 400 ppm) contents, low Y (< 18 ppm), Yb (< 1.9 ppm) and $(^{87}Sr/^{86}Sr)_i$ values (< 0.704), and a lack of Eu anomaly, which were interpreted as the products of partial melting of basaltic slab subducted beneath the mantle wedge (Defant and Drummond, 1990; Drummond and Defant, 1990). Later, other scholars also recognized many intermediate-felsic igneous rocks with the above characteristics (Chung et al., 2003; Tulloch and Kimbrough, 2003), namely adakitic rock, which were considered to be formed via high-pressure partial melting of continental crust. The Yuanzhuding and Dexing porphyries have high La contents (16.3–55.3 ppm) and $(La/Yb)_N$ ratios (12.5–37.0), low Y (6.19–17.5 ppm) and Yb (0.62–1.56 ppm) contents, and negligible Eu anomalies (Eu/Eu* = 0.74–1.42; most < 1.10), suggestive of an affinity with adakite or adakitic rock (Fig. 8B).

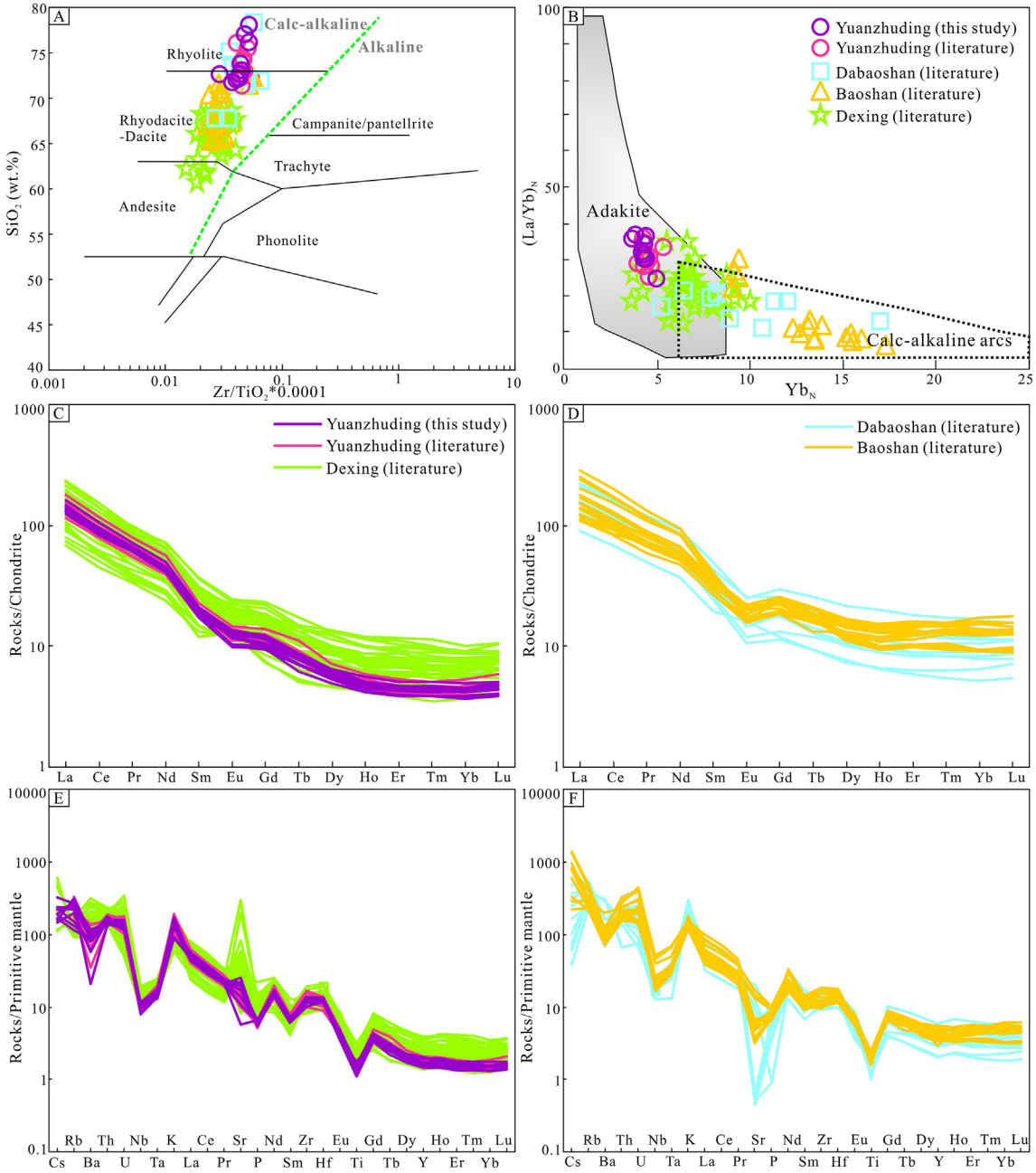

Fig. 8. Geochemistry of the Yuanzhuding, Dabaoshan, Baoshan and Dexing porphyries in the south China. (A) Plot of SiO_2 vs. Zr/TiO_2*0.0001 showing rock classification (Winchester and Floyd, 1977); (B) $(La/Yb)_N$ vs. Yb_N discrimination diagram (Defant and Drummond, 1990; Drummond and Defant, 1990); (C-D) Chondrite-normalized rare earth element (REE) patterns; and (E-F) primitive mantle (PM)–normalized trace-element diagrams (Sun and McDonough, 1989). Data are from this study, Liu et al. (2012), Hou et al. (2013), Xie et al. (2013), Zhong et al. (2013), Wang et al. (2015) and Huang et al. (2017).

5.2.2. Magma source

Studies have suggested that the Yuanzhuding and Dexing porphyries stemmed from the partial melting of subducted oceanic slab (e.g., Zhang et al., 2013). The adakites formed in this way feature depleted Sr-Nd-Hf isotopes, high Na_2O, Mg#, Cr and Ni contents, and low Th and Th/Ce values (Kelemen et al., 2003; Plank, 2005). However, the two porphyries have enriched Nd and Hf isotopic compositions of −3.58 to 0.60 and 0.86 to 7.08 respectively and high Th and Th/Ce values of 11.0–20.0 and 0.18–0.65 respectively (Fig. 10A and B), which demonstrate that they were not sourced from a subducted oceanic slab. Some authors also proposed that the high-pressure partial melting (> 45 km) of thickened or foundered lower crust with a residue of garnet in the source produced these adakitic rocks (Wang et al., 2006; Hou et al., 2013). Experimental petrology has shown that the garnet has significantly higher partition coefficients of HREEs (Er, Tm, Yb and Lu) than middle REEs (MREEs) and LREEs (Rollinson, 1993), and therefore, the $(Gd/Yb)_N$ ratios and REE patterns of porphyries can be used to check whether the garnet is left in magmatic source. The melts generated via the above mechanism commonly have extremely HREE-depleted, "J-shaped" REE patterns and high $(Gd/Yb)_N$ ratios up to 5.8 (Huang and He, 2010; Moyen and Martin, 2012; Ren et al., 2018). However, the Yuanzhuding and Dexing porphyries are devoid of "J-shaped" REE patterns (Fig. 8C) and have low $(Gd/Yb)_N$ ratios (1.84–2.90), which indicates that they were not formed by the partial melting of thickened or foundered lower crust.

Three end members of Mesozoic mantle with distinct elemental and isotopic characteristics have been recognized in this area (Figs. 9A, 10C and D; Wang et al., 2003, 2008a; Li et al., 2004b): (1) asthenospheric

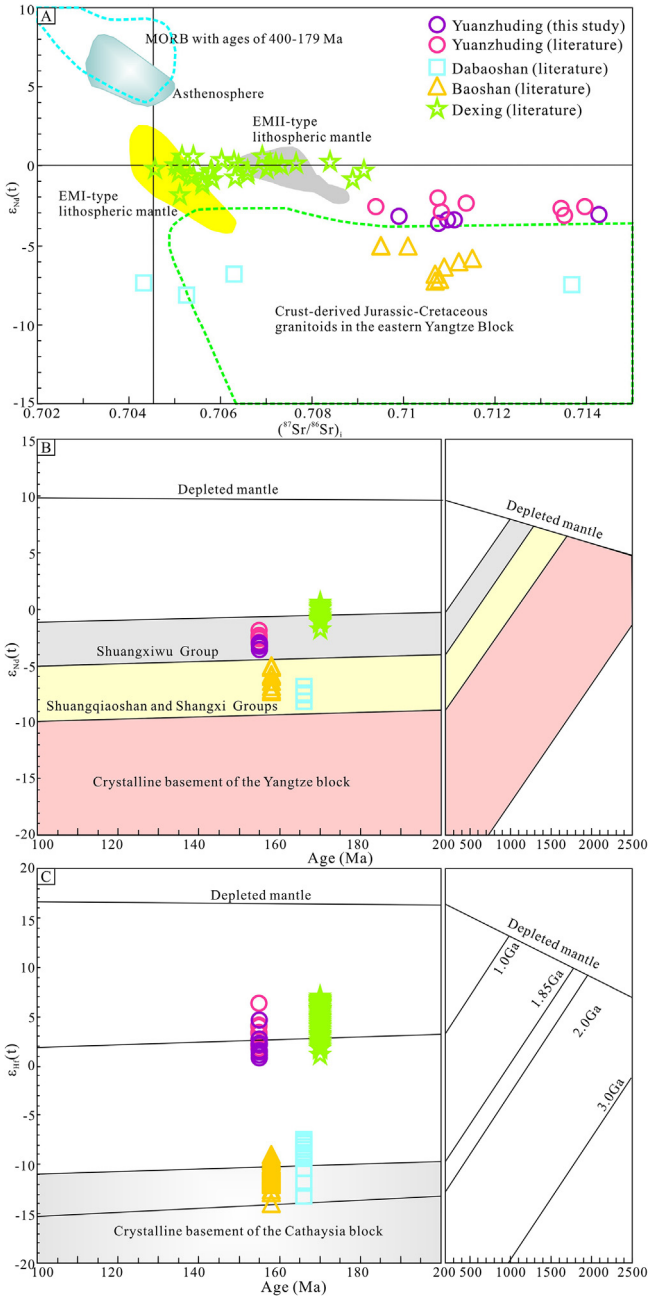

Fig. 9. Comparison of Sr, Nd, and Hf isotopic features for the Yuanzhuding, Dexing, Baoshan and Dabaoshan porphyries, contemporaneous mafic rocks and main crust reservoirs in the South China Block, depleted mantle (MORB) (modified from Zhang et al., 2002, Wang et al., 2006). Two important Meso-Neoproterozoic crustal growth events are represented by the Shuangqiaoshan and Shangxi Groups (1400 Ma) and Shuangxiwu Group (1000–875 Ma) in the South China Block. MORB with ages of 400–179 Ma are from Mahoney et al. (1998), Xu et al. (2003), Tribuzio et al. (2004) and Xu and Castillo (2004). Hf isotopic evolution for the basement of Cathaysia Blockt is from Xu et al. (2007). Data are from this study, Wang et al. (2008a, 2015), Liu et al. (2012), Hou et al. (2013), Xie et al. (2013), Zhong et al. (2013) and Huang et al. (2017).

mantle with depleted Sr and Nd isotopes (initial Sr isotopic ratios of 0.703128–0.704879 and Nd isotopes of 3.99–8.00); (2) EMI-type lithospheric mantle beneath the Yangtz Block featuring enrichment of LREEs and LILEs, depletion of HREEs and HFSEs (especially Nb and Ta) and enriched isotopes (initial Sr isotopic ratios of 0.704341–0.706951 and Nd isotopes of −0.75 to −3.75); (3) EMII-type lithospheric mantle beneath the Cathaysia Block featured by enrichment of LREEs, depletion of HREEs, absence of the negative Nb and Ta anomalies, and enriched isotopes (initial Sr isotopic ratios of 0.706007–0.708665 and Nd isotopes of −2.04 to 1.05). The mafic rocks from EMI- and EMII-type mantle have ages of 125–170 Ma and Nd isotopes of −3.75 to 1.05, which are similar to those of the Yuanzhuding and Dexing porphyries (Fig. 9A). This likely indicates their close genetic link. In fact, some scholars have suggested that the fractional crystallization of enriched-mantle-derived hydrous magmas is a major mechanism forming adakitic rocks (Ma et al., 2016; Dai et al., 2017). The H_2O-rich mafic to intermediate magma can suppress plagioclase fractionation and facilitate hornblende fractionation, thus yielding plagioclase-free residual cumulate and adakitic melt with listric-shaped REE patterns (Carmichael, 2002; Richards and Kerrich, 2007). Different from those from EMII-type mantle, the the REE and muti-element plots of the Yuanzhuding and Dexing porphyries are parallel to those of mafic rocks from EMI-type mantle (Fig. 10C and D), which indicates that the porphyries evolved from EMI-type-mantle-derived mafic rocks. This inference can also be supported by: 1) the porphyries and EMI-type-mantle-derived mafic rocks show significantly negative Nb and Ta anomalies, whereas the EMII-type-mantle-derived mafic rocks do not (Fig. 10D); 2) the major and trace elements of the porphyries and EMI-type-mantle-derived mafic rocks present continuous variations in the Harker diagrams, whereas the EMII-type-mantle-derived mafic rocks do not (Fig. 11A–I).

5.2.3. Fractionation and crustal assimilation

The detailed magmatic evolution, involving fractional crystallization and crustal contamination from EMI-type-mantle-derived mafic rocks to Yuanzhuding and Dexing porphyries, is discussed as follows:

(1) The decreased TiO_2 and Cr with increasing SiO_2 (Fig. 11A and D) suggest fractionation of mafic minerals such as pyroxene, hornblende, biotite and Fe-Ti oxides. Moreover, the bivariate diagram between V and Cr indicates that the evolution from mafic rocks to Dexing porphyry was mainly driven by fractionation of clinopyroxenite, hornblende and biotite, while the evolution from Dexing to Yuanzhuding porphyries by hornblende, biotite and Fe-Ti oxides (Fig. 11J). The fractionation of hornblende and biotite is also consistent with: 1) the decreased trends of Ba, Y and Yb with increasing SiO_2 (Fig. 11E, G and I); (2) the enhanced listric-shaped REE patterns from Dexing to Yuanzhuding porphyries (Richards and Kerrich, 2007; Fig. 8C).

(2) The increased Al_2O_3 with increasing SiO_2 from mafic rocks to Dexing porphyry is consistent with fractionation of mafic minerals, and the decreased trend from Dexing to Yuanzhuding porphyries suggests feldspar fractionation (Fig. 11B). The absence of Eu anomaly in mafic rocks and porphyries can be ascribed to: 1) Eu exists mainly as trivalent rather than bivalent in the oxidized and H_2O-rich magma, as evidenced by the ubiquitous hornblendes, Fe–Ti oxides and titanites (Wang et al., 2003, 2008a) and high zircon Ce^{4+}/Ce^{3+} and Eu_N/Eu_N^* ratios in the mafic rocks and adakitic porphyries (Fig. 6D), which suppresses the incorporation of Eu into plagioclase (Jiang et al., 2013); 2) hornblende fractionation can lead to positive Eu anomaly (Fowler et al., 2008).

(3) The decreased P_2O_5 with an increase in SiO_2 indicates apatite fractionation (Fig. 11C), while the positive correlation between Nb and TiO_2 illustrates titanite fractionation (Fig. 11K).

(4) The horizontal trend of Zr with an increase in SiO_2 demonstrates that there is no zircon fractionation (Fig. 11F).

(5) The Dexing porphyry has Nd isotopes similar to EMI-type-mantle-derived mafic rocks, suggestive of negligible crustal contamination. However, the slightly lower Nd isotopes of Yuanzhuding porphyry than Dexing porphyry and EMI-type-mantle-derived mafic rocks demonstrate that they involved a large number of crustal materials, which is consistent with the fact that they contain many xenocrystic zircons (264–711 Ma; Supplementary Table 1).

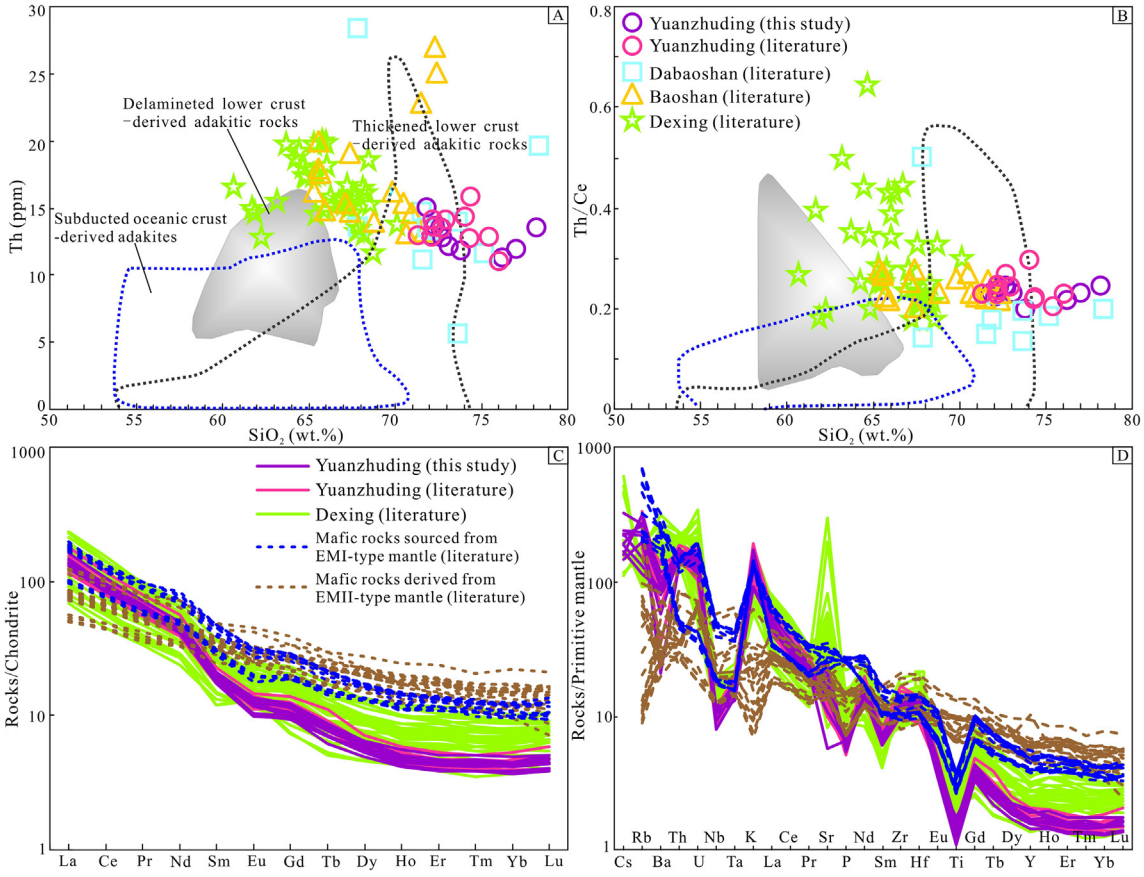

Fig.10. (A and B) Discrimination diagrams of adakite and adakitic rocks with different genetic mechanisms. The fields of thickened and delaminated lower crust-derived adakitic rocks and subducted oceanic crust-derived adakites are from Wang et al. (2006). (C and D) Chondrite-normalized REE and PM–normalized trace-element plots for adakitic pohphyries and contemporaneous mafic rocks from EMI- and EMII-type lithospheric mantle (Sun and McDonough, 1989). Data are from this study, Wang et al. (2003, 2015), Liu et al. (2012), Hou et al. (2013) and Zhong et al. (2013).

As noted above, the hornblende fractionation lowered Y and Yb contents of the Yuanzhuding and Dexing porphyries (Fig. 11E and I), thus yielding adakitic signatures. In this section, the quantitative modeling involving La and Yb is used to simulate the Rayleigh fractional crystallization. The average composition of EMI-type-mantle-derived mafic rocks (La = 33.8 ppm, Yb = 1.86 ppm) is adopted as the primitive magma. Partition coefficients in the basaltic-andesitic and dacitic-rhyolitic melts (Supplementary Table 7; Rollinson, 1993) were used to simulate evolution from mafic rocks to Dexing porphyry, and from Dexing to Yuanzhuding porphyries, respectively. The fractionation equation is expressed as:

$$C = C_0(1 - FC)^{(D-1)}$$

where C and C_0 are element abundances in the resultant and parental magma respectively, D is partition coefficient (Supplementary Table 7), and FC is degree of differentiation (0–1). The results are shown in Fig. 11L, where the trace element trajectory traverses the field of Yuanzhuding and Dexing porphyries. We, therefore, suggest that the adakitic signatures of Yuanzhuding and Dexing porphyries can be formed by 55% and 50% hornblende fractionation of mafic magma respectively.

5.2.4. Mantle metasomatism

The high-Nb (Nb ≥ 20 ppm) and Nb-enriched (7 ppm < Nb < 20 ppm) basalts were mainly proposed to define a group of mafic and alkaline rocks characterized by high HFSEs, TiO_2 and P_2O_5 contents and low LILE/HFSE and HREE /HFSE ratios (Sajona et al., 1996). Given that the hydrous fluids have no ability to transport Nb and Ta, whereas the slab-melts can transport the elements to mantle wedge in the subduction zone (Tatsumi and Nakamura, 1986), the high-Nb and Nb-enriched basalts were commonly thought to be derived from the mantle peridotites hybridized by slab-melts (Benoit et al., 2002; Maury et al., 2009). The Middle-Late Jurassic mafic rocks sourced from EMI-type mantle have high HFSEs and P_2O_5 (0.54–0.59 wt%) contents, especially Nb contents (12.1–36.0 ppm) significantly higher than typical arc basalts (~4 ppm; Liu et al., 2018), low HREEs contents and HREE/HFSE ratios, which resemble those of high-Nb and Nb-enriched basalts (Fig. 12A and B). This indicates that the Middle-Late Jurassic EMI-type lithospheric mantle in the South China Block was enriched by slab-melts.

Besides, the mafic rocks derived from EMI-type mantle also display some chemical characteristics of arc magmatic rocks with their roots in mantle peridotites metasomatized by slab-related hydrous fluids, such as high K_2O (3.62–4.38 wt%), LILEs, K_2O/N_2O (1.53–4.17) and LILE/HFSE values, significantly negative Nb and Ta anomalies (McCulloch and Gamble, 1991). Given that the pelagic sediments commonly contain thousands of ppm of Sr and Ba (Plank and Langmuir 1998), the high Sr and Ba concentrations (459–727 ppm and 1095–2240 ppm respectively) of mafic rocks likely demonstrate that the pelagic-sediments-derived fluids also hybridized EMI-type lithospheric mantle. We, therefore, suggest that the Middle-Late Jurassic EMI-type mantle was likely enriched by basaltic-slab-derived melts and pelagic-sediments-derived fluids, which is also consistent with the positively correlated trends in the plots of Rb/Zr vs. Nb/Zr and Rb/Y vs. Nb/Y (Fig. 12C and D).

In summary, we consider that the Middle-Late Jurassic Yuanzhuding and Dexing porphyries had their origins in an EMI-type lithospheric mantle hybridized by basaltic-slab-derived melts and

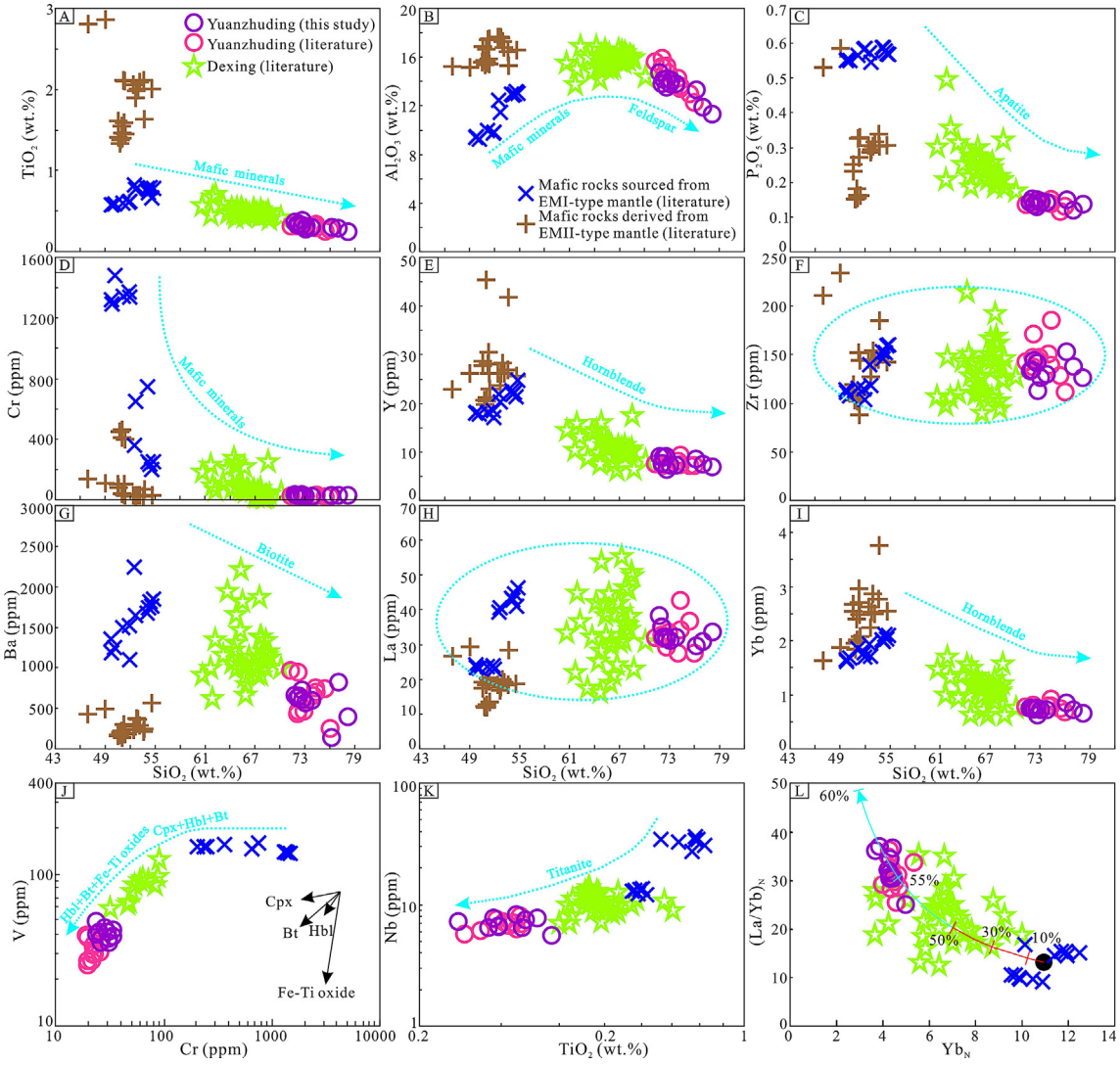

Fig. 11. Harker-type (A–I) and bivariate trace element (J–K) diagrams for the Yuanzhuding and Dexing porphyries and mafic rocks sourced from EMI- and EMII-type lithospheric mantle, with the cyan dotted arrows and mineral names representing magmatic evolution and crystal fractionation respectively. (L) $(La/Yb)_N$ vs. Yb_N plot showing the calculated trend for fractional crystallization from mafic rocks sourced from EMI-type lithospheric mantle to adakitic porphyries. Arrow represents Rayleigh fractional crystallization involving hornblende in a closed system, with tick marks indicating the degree of crystallization. The fractionation trends under the basaltic-andesitic and dacitic-rhyolitic magma are marked with red and cyan solid lines, respectively. Black solid circle represents the average composition of mafic rocks derived from EMI-type mantle. Abbreviations: Cpx = clinopyroxenite; Hbl = hornblende; Bt = biotite. Data are from this study, Wang et al. (2003, 2015), Liu et al. (2012), Hou et al. (2013) and Zhong et al. (2013). (For interpretation of the references to colour in this figure legend, the reader is referred to the web version of this article.)

pelagic-sediments-derived fluids. The Yuanzhuding porphyry was generated via crystal fractionation accompanied by crustal assimilation (AFC processes) of basaltic magma, while the Dexing porphyry was product of fractional crystallization (FC processes). Their adakitic signatures were produced by the 55% and 50% hornblende fractionation of basaltic magma respectively.

5.3. Petrogenesis of low La/Yb Baoshan and Dabaoshan porphyries

The Baoshan and Dabaoshan porphyries display non-adakitic signatures, such as high Y (9.20–27.1 ppm) and Yb (0.89–2.94 ppm) contents, low $(La/Yb)_N$ ratios (6.61–30.6) and Nd-Hf isotopes ($\varepsilon_{Nd}(t) = -8.20$ to -5.00; $\varepsilon_{Hf}(t) = -14.0$ to -7.50) and mildly negative Eu anomaly (Eu/Eu* = 0.57–1.05; most < 0.8), which suggest that they have genetic mechanism and magma source distinct from the contemporaneous adakitic rocks. In general, the granitoids can be formed by crystal fractionation of basaltic magma or partial melting of crustal materials (Nandedkar et al., 2014; Moyen et al., 2017). The Nd isotopes of Baoshan and Dabaoshan porphyries are distinct from the contemporaneous mafic rocks (Fig. 9A), which demonstrates that they were not sourced from mantle. The Archean crystalline basement of Yangtze Block has significantly lower Nd isotopes ($\varepsilon_{Nd}(t) < -10$) than the Baoshan and Dabaoshan porphyries (Fig. 9B; $\varepsilon_{Nd}(t) = -8.20$ to -5.00), thus it can not be the magma source of low La/Yb porphyries. The Nd and Hf isotopes of porphyries fall in the field of Proterozoic crustal materials of Yangtze and Cathaysia Blocks (Fig. 9B and C), suggestive of their origins in the Proterozoic crust of South China Block.

The mafic microgranular enclaves (MMEs) widely distributed in the Baoshan porphyry have Nd isotopes ($\varepsilon_{Nd}(t) = -1.9$ to -2.1; Xie et al., 2013) similar to mafic rocks from EMI-type mantle. The oxygen fugacity of Baoshan porphyry is slightly lower than adaktic porphyries, but higher than ore-barren intrusions from northern Chile (Fig. 6D). As mentioned above, the Middle-Late Jurassic EMI-type-mantle-derived mafic rocks and adakitic porphyries are oxidized and H_2O-rich. Besides, the zircon trace element analyses have demonstrated that the Proterozoic crust in this area has low oxygen fugacity (Zhang et al., 2017;

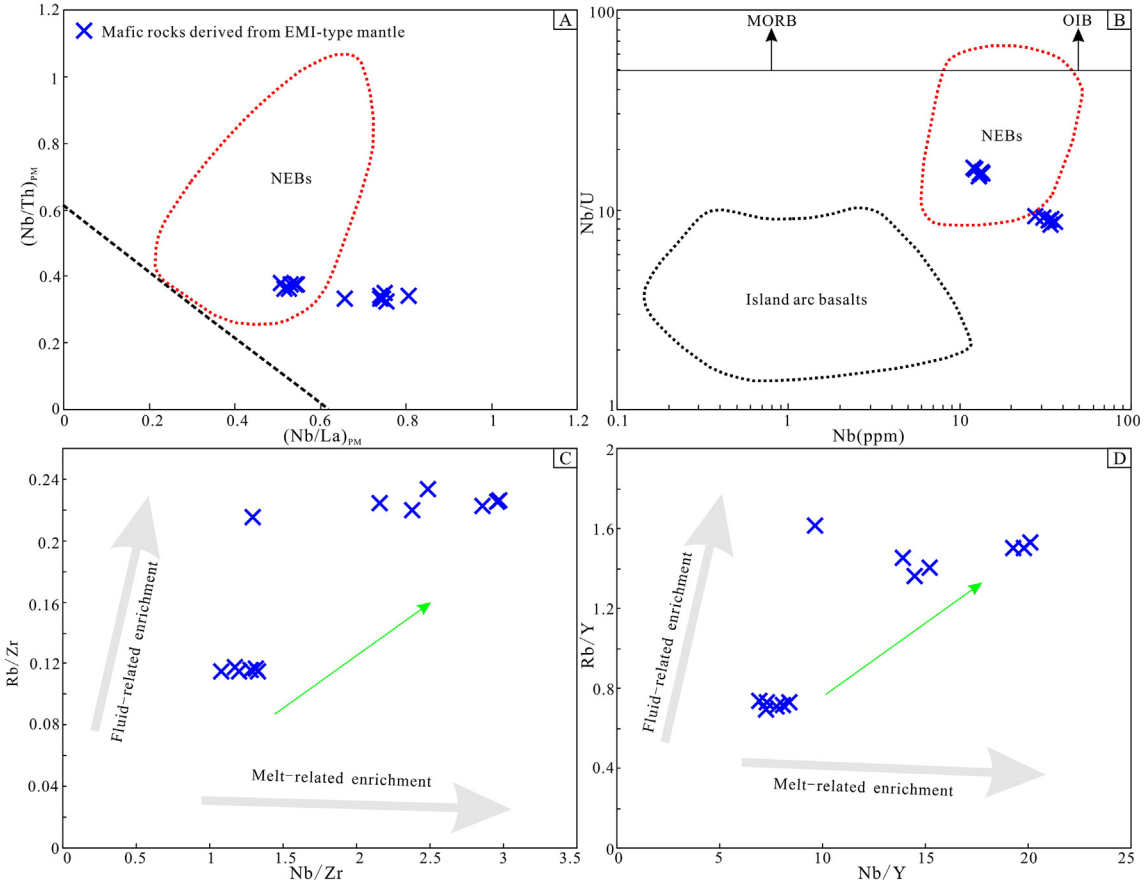

Fig. 12. (A and B) Discrimination diagrams of Nb-enriched basalts (NEBs) (Kepezhinskas et al., 1996; Aguillón-Robles et al., 2001). (C and D) Plots of Rb/Zr vs. Nb/Zr and Rb/Y vs. Nb/Y. Dashed line in (A) discriminate NEBs from arc magmatic rocks (Polat and Kerrich, 2001). Data are from Wang et al. (2003).

ΔFMQ = −2.4 to +0.7). Therefore, the voluminous MMEs and oxidized signature of the Baoshan porphyry indicate that it stemmed from magma mixing between crustal melts and EMI-type-mantle-derived mafic magma. The decreased TiO_2 with an increase in SiO_2 for the Baoshan porphyry (Fig. 13A) indicates fractionation of hornblende and biotite, which are consistent with the concomitantly decreased Cr and Ni contents (Fig. 13D). The decreased trends of Al_2O_3 and P_2O_5 with increasing SiO_2 (Fig. 13B and C) demonstrate feldspar and apatite fractionation. Besides, the bivariate trace element plots (Fig. 13E–G) indicate the fractionation of zircon and apatite.

The Dabaoshan porphyry displays bimodally distributed zircon Ce^{4+}/Ce^{3+} and Eu_N/Eu_N^* ratios, with high ratios close to adakitic porphyries but low values plotting in ore-barren intrusions (Fig. 6D). Besides, the U vs. Ce^{4+}/Ce^{3+} plot for zircon also has bimodal distribution (Fig. 13H). The above bimodal distribution likely indicates that the continental-crust-derived Dabaoshan porphyry also involved EMI-type-mantle-derived mafic magma, which is consistent with the fact that its Nd-Hf isotopes are similar to Baoshan porphyry. A lack of MMEs in the Dabaoshan porphyry can be attributed to the weak involvement of mafic magma. The decreased TiO_2 with increasing SiO_2 for the Dabaoshan porphyry (Fig. 13A) indicates fractionation of hornblende and biotite, which are consistent with the concomitantly decreased Cr and Ni contents (Fig. 13D). The decreased trends of Al_2O_3 and P_2O_5 with increasing SiO_2 (Fig. 13B and C) demonstrate feldspar and apatite fractionation. The concomitantly decreased Nb and TiO_2 (Fig. 13E) suggests titanite fractionation. In addition, the plots of Ce vs. Zr and Ce vs. Nb (Fig. 13F and G) further indicate the fractionation of titanite, zircon and apatite.

In conclusion, we suggest that the Baoshan porphyry was produced by magma mixing between crustal melt and EMI-type-mantle-derived mafic magma and subsequent fractional crystallization. The Dabaoshan porphyry evolved from crustal melts via magmatic differentiation with input of minor mafic magma.

5.4. Geodynamic and metallogenic implications: an integrated model

Porphyry copper deposits were commonly found in subduction environment (Chiaradia, 2014) and interpreted to be formed by: 1) partial melting of subducted basaltic slab with high Cu contents (Wilkinson, 2013); (2) the normal arc magma extracting Cu from the mantle under a variety of coupled geological conditions, such as tectonic mechanism, host rocks, fractional crystallization and volatile exsolution (Richards, 2013). In contrast, the porphyry deposits in a post-subduction setting are commonly associated with the ancient subduction events that formed Cu-rich mantle and had ceased before the ore-related magmatism (Richards, 2009; Pettke et al., 2010). The Middle-Late Jurassic giant porphyry deposits along the Qin-Hang belt were formed in the interior of South China Block, thus, their genetic studies may provide a new perspective for exploring the geodynamic models and factors controlling the formation of porphyry deposits with different element associations.

5.4.1. Geodynamic model

Some scholars argued that the Middle-Late Jurassic porphyry deposits along the Qin-Hang belt were mainly controlled by the partial melting of thickened or foundered lower crust (Wang et al., 2006; Hou et al., 2013). However, as mentioned above, our new genetic models do not support this inference. Our models reveal that the Jurassic lithospheric mantle in this area was metasomatized by basaltic-slab-derived melts and pelagic-sediments-derived fluids. Studies have demonstrated

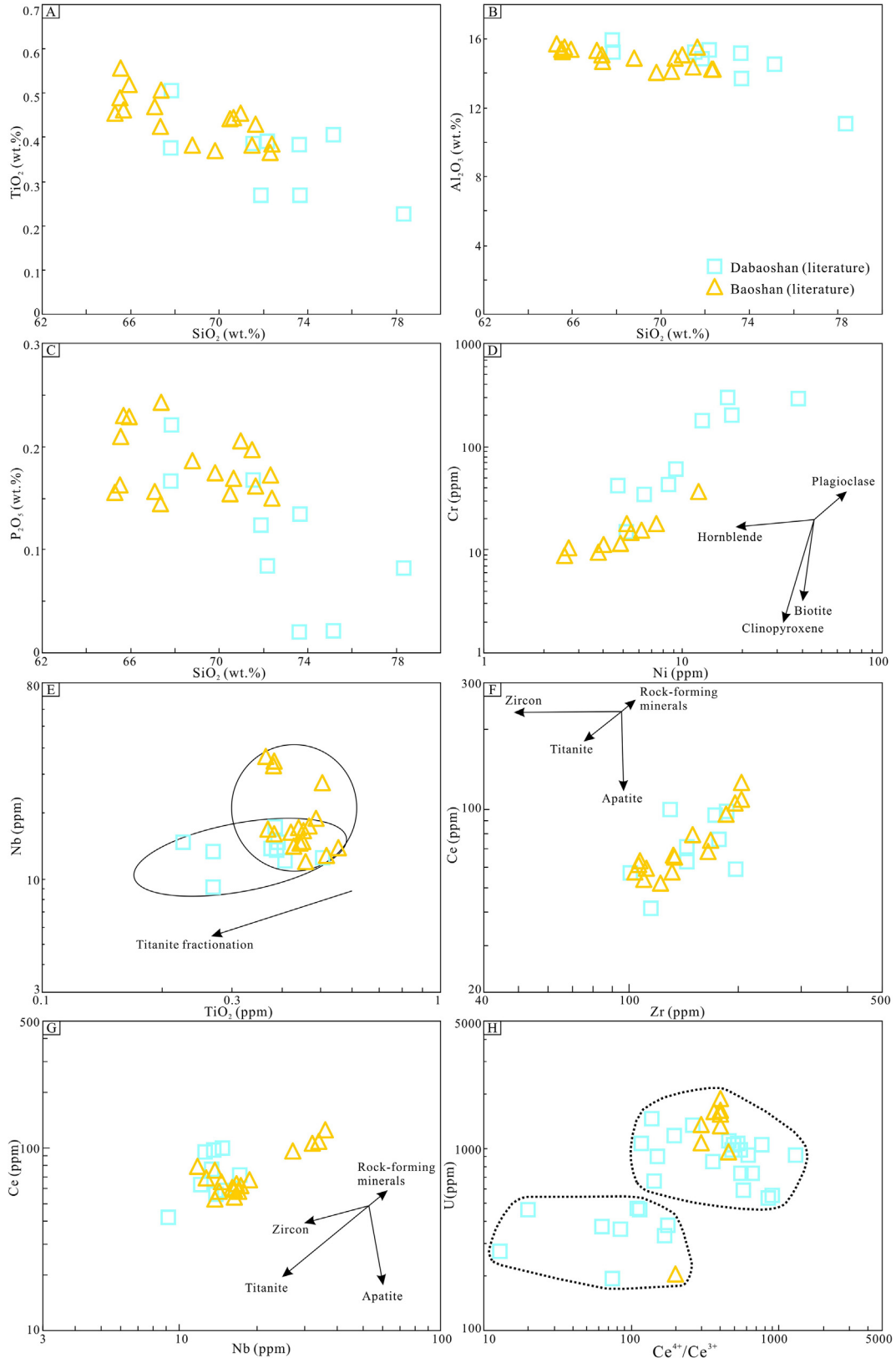

Fig. 13. Harker-type (A–C), whole-rock bivariate trace element (D–G) and zircon trace element plots (H) for the Baoshan and Dabaoshan porphyries. Trends shown in (D, F, G) are from Fowler et al. (2008). Data are from Xie et al. (2013) and Huang et al. (2017).

that the Neoproterozoic arc-related rocks and ophiolites existed in the Qin-Hang belt and Jiangnan orogen respectively, which indicate that the Yangtze and Cathaysia Blocks experienced Neoproterozoic continental collision (Zhao et al., 2018). From then on, the Yangtze and Cathaysia Blocks have been consolidated into a single terrane until the Triassic-Jurassic subduction of the Paleo-Pacific plate beneath the South China Block (Wang et al., 2006; Li et al., 2019b). The Middle-Late Jurassic formation ages of the adakitic Yuanzhuding and Dexing

porphyries (ca. 155–170 Ma; Wang et al., 2015) further suggest that the Middle-Late Jurassic EMI-type lithospheric mantle likely experienced Neoproterozoic and Triassic-Jurassic mantle metasomatism. The Neoproterozoic arc magmatic rocks (the Shuangxiwu Group) are featured by low Nb (1.98–9.21 ppm; most ≤ 7 ppm) and Ta (0.12–0.68 ppm; most ≤ 0.4 ppm) contents, enrichment in LILEs and LREEs, depletion in HFSEs and HREEs, which indicate that their mantle source was enriched by slab-derived fluids (Li et al., 2009). We, therefore, propose that the Middle-Late Jurassic lithospheric mantle beneath the Qin-Hang belt underwent two-stage mantle metasomatism. The one related to slab-derived fluids might happen in Neoproterozoic and Triassic-Jurassic, while the other associated with basaltic-slab-melts could only occur in Triassic-Jurassic. Adakites were initially considered to be derived from the partial melting of juvenile basaltic slab with high temperatures in the plate convergent margin (Defant and Drummond, 1990; Drummond and Defant, 1990), which is in contradiction to the fact that the Middle-Late Jurassic porphyry deposits are over 1000 km away from the subduction zones. However, the occurrence of slab melting indeed requires a significant geodynamic change, possibly related to the opening of slab window, during the subduction of Paleo-Pacifc plate. Early geologists have put forward an alternative model: ridge subduction (Zhang et al., 2013). As shown in Fig. 1, the facts that the Qin-Hang porphyry metallogenic belt extends NNE and that the Dexing porphyry in the northeast end of this belt has older ages than that in the southwest part require a southwestward ridge subduction. However, the southwestward subduction of Paleo-Pacific plate only occurred in the Early Triassic and Early Cretaceous (Ling et al., 2009; Li et al., 2013).

The Yuanzhuding and Dexing porphyries and EMI-type-mantle-derived mafic rocks have ages of 145–170 Ma (Wang et al., 2003, 2008a), which indicates that the Paleo-Pacific slab has subducted beneath the interior of South China Block (Qin-Hang belt) before Middle Jurassic (ca. 170 Ma). Besides, the progressively northwestward subduction of Paleo-Pacific slab from Triassic to Middle-Late Jurassic can also be supported by the following: (1) strike-slip faults with ages of 200–135 Ma and 160–135 Ma become progressively younger from east to west part of North China Craton and South China Block respectively (Li et al., 2018b); (2) metamorphism and magmatism with ages of ca. 265–190 Ma become progressively younger from east to west part of South China Block (Li and Li, 2007); (3) foreland basin and fold-and-thrust belt migrated towards the interior of South China Block for ~600 km from ca. 265 Ma to ca. 190 Ma (Li, 1998; Li and Li, 2007). Studies have shown that the flat-slab subduction can extend over 1200 km into the continental interior and trigger strong compressional deformation (Livaccari et al., 1981; Jordan et al., 1983). Given that the Middle-Late Jurassic porphyry deposits are over 1000 km away from the subduction zone, we suggest that the northwestward flat-slab subduction of Paleo-Pacific crust beneath the interior of South China Block would be required (Fig. 14A; Wang et al., 2008b). The partial melting of basaltic slab with ages of ca.145–170 Ma also indicates a significant extensional setting, possibly related to slab break-off or slab roll-back. However, the slab-roll back can lead to a coastward-younging trend, which is not the case for the Middle-Late Jurassic rocks. We, therefore, suggest that the slab break-off beneath Qin-Hang belt is the most likely mechanism (Fig. 14B and C), which is also supported by the magmatic and sedimentary records: 1) the Middle-Late Jurassic mafic rock with depleted and enriched isotopes emplaced along the Qin-Hang belt (Wang et al., 2003, 2008a); (2) the shallow terrestrial basin and marine sediments with ages of ca.210–190 Ma occurred along the Qin-Hang belt (Li and Li, 2007).

5.4.2. Metallogenic model

The fertile adakites formed via slab melting are commonly thought to be the most likely magma favoring porphyry Cu mineralization (Sun et al., 2013), which was mainly ascribed to the following factors: (1) slab-melts are significantly oxidized and sulfur-rich, which can not only yield oxidized sulfides containing chalcophile elements, thus extracting metals from mantle wedge, but also suppress the precipitation of sulfide during magmatic differentiation, thus resulting in the enrichment of metallogenic elements in the late-stage of magmatic evolution (Mungall, 2002; Sun et al., 2007; Liang et al., 2018); (2) they are unusually water-rich, facilitating volatile exsolution during the late-stage of magmatic evolution (Sajona and Maury, 1998); (3) they contain much higher Cu abundance (~100 ppm) than the mantle (~30 ppm) and continental crust (~27 ppm) (Sun et al., 2010).

The Middle-Late Jurassic northwestward flat-slab subduction and related slab break-off triggered asthenosphere upwelling and subsequent partial melting, thus forming adakitic slab-melts with high Cu, H_2O and S contents and oxidized characteristic. These melts would ascend and hybridize the overlying lithospheric mantle previously incorporating slab-related hydrous fluids. Besides, the asthenosphere upwelling could elevate thermal gradient of lithospheric mantle, thus forming basaltic magma with high Cu, H_2O and S contents and oxidized feature. Moreover, the flat-slab subduction can yield compressional environment, which is favorable for the formation of a non-erupting and closed magma chamber in the upper plate, and therefore, sulfur could be precipitated as sulfides and sulfates, rather than being discharged as gas SO_2 (Oyarzun et al., 2002). In this case, the basaltic magma derived from a fertile mantle could experience AFC and FC processes in a closed magma chamber, thus forming Yuanzhuding and Dexing porphyries. Given the high volatile/melt partition coefficients of Cu and Au, especially the volatile containing more sulfurs (Simon et al., 2006; Zajacz et al., 2012), the further volatile exsolution of Dexing porphyry would generate Cu-Au-dominated Cu-Au-Mo mineralization, whilst the Yuanzhuding porphyry incorporating some Mo-rich crustal materials are favorable for Cu-Mo-dominated mineralization (Fig. 14D; Supplementary Table 8).

Different from these models, the Baoshan and Dabaoshan porphyries show a crustal origin, with involvement of voluminous and minor enriched-mantle-derived mafic magma respectively. In the flat-slab subduction setting, slab break-off and melting will occur in the interior of South China Block. The thick “intraplate” crust and a thicker one due to flat-slab subduction are different from the thin crust of continental margin hosting a large number of porphyry Cu-Au deposits. The thick crust and compressional environment are favorable for the formation of crustal melts with input of voluminous and minor mafic magma in a closed magma chamber, thus forming Baoshan and Dabaoshan porphyries. Besides, the input of EMI-type-mantle-derived mafic magma can provide Cu, H_2O, S and oxidized magma for continental-crust-derived porphyries, which are essential for the formation of porphyry deposits (Sun et al., 2015). We, therefore, suggest that the fractional crystallization and volatile exsolution of the Baoshan porphyry incorporating voluminous EMI-type-mantle-derived mafic magma produced Pb-Zn-dominated Pb-Zn-Cu-Mo mineralization, while the Dabaoshan porphyry containing minor mafic magma generated Mo-W-dominated Mo-W-Pb-Zn mineralization (Fig. 14D; Supplementary Table 8).

In conclusion, we suggest that the “intraplate” porphyry deposits are closely related to an enriched mantle hybridized by fluids and slab-melts and controlled by flat-slab subduction and related slab break-off (Fig. 14A–C). The above geodynamic mechanism induced complex crust-mantle interaction, thus forming the “intraplate” porphyry deposits with different element associations (Fig. 14D). As the magma sources of ore-forming porphyries transform from enriched-mantle- to continental-crust-dominated materials, the metallogenic elements of “intraplate” porphyry deposits will change from Cu-Au-Mo- to Mo-W-Pb-Zn-dominated mineralization (Supplementary Table 8).

6. Conclusion

The comprehensive geochronological, mineralogical, elemental and isotopic investigation into the Middle-Late Jurassic porphyry deposits

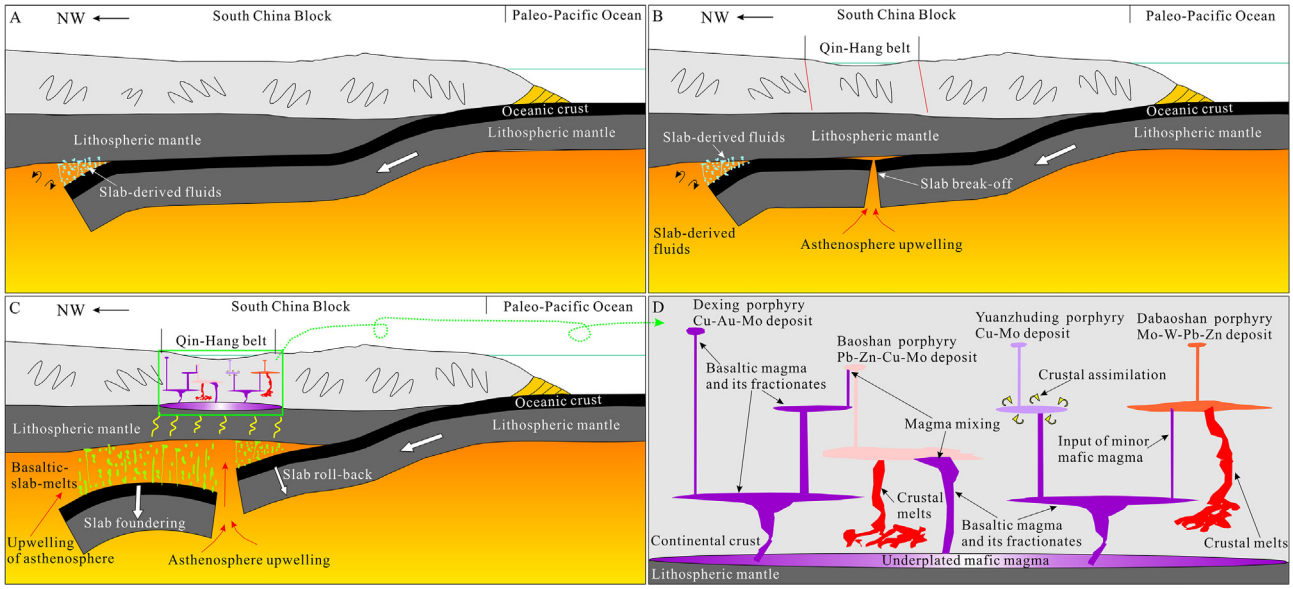

Fig. 14. Cartoons showing the Triassic and Middle-Late Jurassic northwestward flat-slab subduction of Paleo-Pacific slab beneath the interior of South China Block (modified from Li and Li, 2007) and the genesis of "intraplate" porphyry deposits along the Qin-Hang belt: (A) the Triassic-Early Jurassic northwestward flat-slab subduction of Paleo-Pacific slab; (B and C) slab break-off and foundering of Paleo-Pacific oceanic crust along the Qin-Hang belt during Middle-Late Jurassic; (D) genesis of "intraplate" porphyry deposits.

along the Qin-Hang belt in the interior of South China Block reveals a new magmatic and metallogenic model. The high La/Yb Yuanzhuding and Dexing porphyries were formed via AFC and FC processes of basaltic magma derived from an EMI-type lithospheric mantle incorporating fluids and slab-melts respectively. Their adakitic signatures can be attributed to hornblende fractionation. In contrast, the low La/Yb Baoshan and Dabaoshan porphyries stemmed from FC processes of partial melts of the Proterozoic crustal rocks, with involvement of voluminous and a little EMI-type-mantle-derived basaltic magma respectively. Integrated with the Triassic-Jurassic geological records in the region, the petrogenesis of ore-forming porphyries indicates that the "intraplate" porphyry deposits were controlled by the northwestward flat-slab subduction and related slab break-off. We, therefore, propose that the "intraplate" porphyry deposits with different element associations result from complicated crust-mantle interaction in the thick "intraplate" crust, and that their metallogenic elements will change from Cu-Au-Mo- to Mo-W-Pb-Zn-dominated mineralization with the transformation of magma sources from enriched-mantle- to continental-crust-dominated materials.

Declaration of Competing Interest

The authors declare that they have no known competing financial interests or personal relationships that could have appeared to influence the work reported in this paper.

Acknowledgement

This study was supported by the National Key R&D Program of China (2016YFC0600407) and the National Natural Science Foundation of China (41772065). We appreciate the constructive review by professor Xiaoyong Yang and comments from two anonymous reviewers. This is contribution No. IS-2848 from GIGCAS.

Appendix A. Supplementary data

Supplementary data to this article can be found online at https://doi.org/10.1016/j.oregeorev.2020.103574.

References

Aguillón-Robles, A., Calmus, T., Benoit, M., Bellon, H., Maury, R., Cotton, J., Bourgois, J., Michard, F., 2001. Late Miocene adakites and Nb–enriched basalts from Vizcaino Peninsula, Mexico: indicators of East Pacific Rise subduction below southern Baja California. Geology 29, 531–534.

Ballard, J.R., Palin, M.J., Campbell, I.H., 2002. Relative oxidation states of magmas inferred from Ce(IV)/Ce(III) in zircon: application to porphyry copper deposits of northern Chile. Contrib. Mineral. Petrol. 144, 347–364.

Benoit, M., Aguillón-Robles, A., Calmus, T., Maury, R.C., Bellon, H., Cotten, J., Bourgois, J., Michaud, F., 2002. Geochemical diversity of late Miocene volcanism in southern Baja California, México: implication of mantle and crustal sources during the opening of an asthenospheric window. J. Geol. 110, 627–648.

Camus, F., Dilles, J.H., 2001. A special issue devoted to porphyry copper deposits of northern Chile – preface. Econ. Geol. 96, 233–237.

Carmichael, I.S.E., 2002. The andesite aqueduct: perspectives on the evolution of intermediate magmatism in west–central (105–99°W) Mexico. Contrib. Mineral. Petrol. 143, 641–663.

Carter, A., Roques, D., Bristow, C., Kinny, P., 2001. Understanding Mesozoic accretion in Southeast Asia: significance of Triassic thermotectonism. Geology 29, 211–214.

Charvet, J., 2013. The Neoproterozoic-Early Paleozoic tectonic evolution of the South China Block: an overview. J. Asian Earth Sci. 74, 198–209.

Chen, F.W., Li, H.Q., Wang, D.H., Xiao, G.M., Yang, X.J., Gao, Y.W., Mei, Y.P., Lin, X.G., 2012. Geological characteristics and diagenetic–metallogenic chorological study of the Yuanzhuding porphyry Cu–Mo deposit, western Guangdong Province. Acta Geol. Sin. 86, 1298–1305 (in Chinese with English abstract).

Chen, J.F., Jahn, B.M., 1998. Crustal evolution of southeastern China: Nd and Sr isotopic evidence. Tectonophysics 284, 101–133.

Chen, X.L., Richards, J.P., Liang, H.Y., Zou, Y.Q., Zhang, J., Huang, W.T., Ren, L., Wang, F.Y., 2019. Contrasting arc magma fertilities in the Gangdese belt, Southern Tibet: evidence from geochemical variations of Jurassic volcanic rocks. Lithos 324–325, 789–802.

Chen, Y.J., Wang, P., Li, N., Yang, Y.F., Pirajno, F., 2016. The collision–type porphyry Mo deposits in Dabie Shan, China. Ore Geol. Rev. 81, 405–430.

Chiaradia, M., 2014. Copper enrichment in arc magmas controlled by overriding plate thickness. Nat. Geosci. 7, 43–46.

Chu, K.L., 2013. The diagenesis and metallogeneses studies on Yuanzhuding porphyry Cu–Mo deposit in Guangdong, PhD Thesis. Chinese Academy of Geological Sciences, Beijing, pp. 1–112 (in Chinese with English abstract).

Chu, K.L., Mao, J.W., Chen, M.H., Zhao, J., Yu, C.F., Lin, L.Z., Lin, X.G., 2013. Source of metallogenic materials and ore–forming fluids, and metallogenic mechanism of the Yuanzhuding porphyry Cu–Mo deposit, western Guangdong Province, South China. Earth Sci. Front. 20, 115–125 (in Chinese with English abstract).

Chung, S.L., Liu, D.Y., Ji, J.Q., Chu, M.F., Lee, H.Y., Wen, D.J., Lo, C.H., Lee, T.Y., Qian, Q., Zhang, Q., 2003. Adakites from continental collision zones: melting of thickened lower crust beneath southern Tibet. Geology 31, 1021–1024.

Dai, H.K., Zheng, J.P., Zhou, X., Griffin, W.L., 2017. Generation of continental adakitic rocks: crystallization modeling with variable bulk partition coefficients. Lithos 272–273, 222–231.

Defant, M.J., Drummond, M.S., 1990. Derivation of some modern arc magmas by melting of young subducted lithosphere. Nature 347, 662–665.

Drummond, M.S., Defant, M.J., 1990. A model for trondhjemite–tonalite–dacite genesis and crustal growth via slab melting: Archaean to modern comparisions. J. Geophys. Res. 95, 21503–21521.
Du, A.D., Qu, W.J., Li, C., Yang, G., 2009. A review on the development of Re–Os isotopic dating methods and techniques. Rock Miner. Anal. 28, 288–304 (in Chinese with English abstract).
Ernst, W.G., Tsujimori, T., Zhang, R., Liou, J.G., 2007. Permo-Triassic collision, subduction–zone metamorphism, and tectonic exhumation along the east Asian continental margin. Annu. Rev. Earth Planet. Sci. 35, 73–110.
Fowler, M.B., Kocks, H., Darbyshire, D.P.F., Greenwood, P.B., 2008. Petrogenesis of high Ba–Sr plutons from the Northern Highlands Terrane of the British Caledonian Province. Lithos 105, 129–148.
Goodell, P.C., Gilder, S., Fang, X., 1991. A preliminary description of the Gan-Hang failed rift, southeastern China. Tectonophysics 197, 245–255.
Hou, Z.Q., Pan, X.F., Li, Q.Y., Yang, Z.M., Song, Y.C., 2013. The giant Dexing porphyry CuMo–Au deposit in east China: product of melting of juvenile lower crust in an intracontinental setting. Mineral. Depos. 48, 1019–1045.
Hou, Z.Q., Yang, Z.M., Lu, Y.J., Kemp, A., Zheng, Y.C., Li, Q.Y., Tang, J.X., Yang, Z.S., Duan, L.F., 2015. A genetic linkage between subduction- and collision-related porphyry Cu deposits in continental collision zones. Geology 43, 247–250.
Hou, Z.Q., Yang, Z.M., Qu, X.M., Meng, X.J., Li, Z.Q., Beaudoin, G., Rui, Z.Y., Gao, Y.F., Zaw, K., 2009. The Miocene Gangdese porphyry copper belt generated during post–collisional extension in the Tibetan Orogen. Ore Geol. Rev. 36, 25–51.
Huang, F., He, Y.S., 2010. Partial melting of the dry mafic continental crust: Implications for petrogenesis of C–type adakites. Chin. Sci. Bull. 55, 1255–1267 (in Chinese).
Huang, W.T., Liang, H.Y., Wu, J., Zou, Y.Q., Zhang, J., 2017. Formation of porphyry Mo deposit in a deep fault zone, example from the Dabaoshan porphyry Mo deposit in northern Guangdong, South China. Ore Geol. Rev. 81, 940–952.
Huang, W.T., Liang, H.Y., Zhang, J., Chen, X.L., Lin, S.P., Zou, Y.Q., Ren, L., Wu, J., Zhang, L.P., 2020. Formation of the Cretaceous skarn Cu–Au deposits of the southern Gangdese belt, Tibet: case studies of the Kelu and Sangbujiala deposits. Ore Geol. Rev. 122, 103481.
Huang, W.T., Liang, H.Y., Zhang, J., Wu, J., Chen, X.L., Ren, L., 2019. Genesis of the Dachang Sn-polymetallic and Baoshan Cu ore deposits, and formation of a Cretaceous Sn-Cu ore belt from southwest China to western Myanmar. Ore Geol. Rev. 112, 103030.
Jiang, C.Z., Wang, Q.F., Li, G.J., Ma, N., Hu, Z.C., 2013. Relative oxidation states of intrusions in Beiya gold–polymetallic deposit in Sanjiang area, Yunnan, SW China. Acta Petrol. Sin. 29, 3925–3936 (in Chinese with English abstract).
Jordan, T.E., Isacks, B.L., Allmendinger, R.W., Brewer, J.A., Ramos, V.A., Ando, C.J., 1983. Andean tectonics related to geometry of subducted Nazca plate. Geol. Soc. Am. Bull. 94, 341–361.
Kelemen, P.B., Yogodzinski, G.M., Scholl, D.W., 2003. Along strike variation in the Aleutian island arc: genesis of high–Mg# andesite and implications for continental crust. In: Eiler, J. (Ed.), Inside the Subduction Factory. Geophysical Monograph, vol. 138. American Geophysical Union, Washington, pp. 223–276.
Kepezhinskas, P.K., Defant, M.J., Drummond, M.S., 1996. Progressive enrichment of island arc mantle by melt–peridotite interaction inferred from Kamchatka xenoliths. Geochim. Cosmochim. Acta 60, 1217–1229.
Li, C.Y., Zhang, H., Wang, F.Y., Liu, J.Q., Sun, Y.L., Hao, X.L., 2012. The formation of the Dabaoshan porphyry molybdenum deposit induced by slab rollback. Lithos 150, 101–110.
Li, H., Kong, H., Zhou, Z.K., Wu, Q.H., Xi, X.S., Gabo-Ratio, J.A.S., 2019a. Ore–forming material sources of the Jurassic Cu–Pb–Zn mineralization in the Qin-Hang ore belt, South China: constraints from S-Pb isotopes. Geochemistry 79, 280–306.
Li, S.Z., Suo, Y.H., Li, X.Y., Wang, Y.M., Cao, X.Z., Wang, P.C., Guo, L.L., Yu, S.Y., Lan, H.Y., Li, S.J., Zhao, S.J., Zhou, Z.Z., Zhen, Z., Zhang, G.W., 2018a. Mesozoic plate subduction in West Pacific and tectono–magmatic response in the East Asian ocean–continent connection zone. Chin. Sci. Bull. 63, 1550–1593 (in Chinese with English abstract).
Li, S.Z., Suo, Y.H., Li, X.Y., Zhou, J., Santosh, M., Wang, P.C., Wang, G.Z., Guo, L.L., Yu, S.Y., Lan, H.Y., Dai, L.M., Zhou, Z.Z., Cao, X.Z., Zhu, J.J., Liu, B., Jiang, S.H., Wang, G., Zhang, G.W., 2019b. Mesozoic tectono–magmatic response in the East Asian ocean–continent connection zone to subduction of the Paleo-Pacifc Plate. Earth Sci. Rev. 192, 91–137.
Li, S.Z., Yu, S., Zhao, S.J., Liu, X., Gong, S.Y., Suo, Y.H., Dai, L.M., Ma, Y., Xu, L.Q., Cao, X.Z., Wang, P.C., Sun, W.J., Yang, C., Zhu, J.J., 2013. Tectonic transition and plate reconstructions of the East Asian Continental Magin. Mar. Geol. Quat. Geol. 33, 65–94 (in Chinese).
Li, X.F., Hua, R.M., Ma, D.S., Xu, J., Zhang, L., Qi, Y.Q., Wu, Y.L., Zhu, Y.T., 2018b. Mesozoic sub–continental lithospheric mantle extension and related porphyry copper mineralization in South China. Acta Petrol. Sin. 35, 76–88 (in Chinese with English abstract).
Li, X.H., Chung, S.L., Zhou, H.W., Lo, C.H., Liu, Y., Chen, C.H., 2004b. Jurassic intraplate magmatism in southern Hunan–eastern Guangxi: 40Ar/39Ar dating, geochemistry, Sr–Nd isotopes and implications for tectonic evolution of SE China. In: Malpas, J., Fletcher, C.J., Aitchison, J.C. Ali, J. (Eds.), Aspects of the Tectonic Evolution of China. Geological Society, London, Special Publications, 226, 193–216.
Li, X.H., Li, W.X., Li, Z.X., Lo, C.H., Wang, J., Ye, M.F., Yang, Y.H., 2009. Amalgamation between the Yangtze and Cathaysia Blocks in South China: constraints from SHRIMP U-Pb zircon ages, geochemistry and Nd–Hf isotopes of the Shuangxiwu volcanic rocks. Precamb. Res. 174, 117–128.
Li, X.H., Li, Z.X., Wingate, M.T.D., Chung, S.L., Liu, T., Lin, G.C., Li, W.X., 2006. Geochemistry of the 755 Ma Mundine Well dyke swarm, northwestern Australia: part of a Neoproterozoic mantle superplume beneath Rodinia? Precamb. Res. 146, 1–15.
Li, X.H., Liu, D.Y., Sun, M., Li, W.X., Liang, X.R., Liu, Y., 2004a. Precise Sm–Nd and U-Pb isotopic dating of the supergiant Shizhuyuan polymetallic deposit and its host granite, SE China. Geol. Mag. 141, 225–231.
Li, X.H., Long, W.G., Li, Q.L., Liu, Y., Zheng, Y.F., Yang, Y.H., Chamberlain, K.R., Wan, D.F., Guo, C.H., Wang, X.C., Tao, H., 2010. Penglai zircon megacrysts: a potential new working reference material for microbeam determination of Hf–O isotopes and U-Pb age. Geostand. Geoanal. Res. 34, 117–134.
Li, Z.X., 1998. Tectonic history of the major East Asian lithospheric blocks since the mid-proterozoic–a synthesis. Am. Geophys. Union Geodyn. Ser. 27, 221–243.
Li, Z.X., Li, X.H., 2007. Formation of the 1300–km–wide intracontinental orogen and postorogenic magmatic province in Mesozoic South China: a flat–slab subduction model. Geology 35, 179–182.
Li, Z.X., Li, X.H., Zhou, H., Kinny, P.D., 2002. Grenvillian continental collision in South China: new SHRIMP U-Pb zircon results and implications for the configuration of Rodinia. Geology 29, 211–214.
Liang, H.Y., Campbell, I.H., Allen, C., Sun, W.D., Liu, C.Q., Yu, H.X., Xie, Y.W., Zhang, Y.Q., 2006. Zircon Ce^{4+}/Ce^{3+} ratios and ages for Yulong ore–bearing porphyries in eastern Tibet. Mineral. Depos. 41, 152–159.
Liang, H.Y., Campbell, I.H., Allen, C.M., Sun, W.D., Yu, H.X., Xie, Y.W., Zhang, Y.Q., 2007. The age of the potassic alkaline igneous rocks along the Ailao Shan-Red River shear zone: implications for the onset age of left–lateral shearing. J. Geol. 115, 231–242.
Liang, H.Y., Sun, W.D., Su, W.C., Zartman, R.E., 2009. Porphyry copper–gold mineralization at Yulong, China, promoted by decreasing redox potential during magnetite alteration. Econ. Geol. 104, 587–596.
Liang, H.Y., Zhang, J., Huang, W.T., Chen, X.L., Ren, L., Li, K.X., Wang, X.Z., 2018. Mechanisms for transform of sulfate in porphyry high oxidized magma to ore–forming sulfur of porphyry Cu (± Au–Mo) deposits and their application. J. Nanjing Univ. (Nat. Sci.) 54, 236–244 (in Chinese with English abstract).
Ling, M.X., Wang, F.Y., Ding, X., Hu, Y.H., Zhou, J.B., Zartman, R.E., Yang, X.Y., Sun, W.D., 2009. Cretaceous ridge subduction along the Lower Yangtze River belt, eastern China. Econ. Geol. 104, 303–321.
Livaccari, R.F., Burke, K., Sengör, A.M.C., 1981. Was the Laramide orogeny related to subduction of an oceanic plateau? Nature 289, 276–278.
Liu, H.C., Xia, X.P., Lai, C.K., Gan, C.S., Zhou, Y.Z., Huangfu, P.P., 2018. Break–away of South China from Gondwana: Insights from the Silurian high–Nb basalts and associated magmatic rocks in the Diancangshan-Ailaoshan fold belt (SW China). Lithos 318–319, 194–208.
Liu, X., Fan, H.R., Santosh, M., Hu, F.F., Yang, K.F., Li, Q.L., Yang, Y.H., Liu, Y.S., 2012. Remelting of Neoproterozoic relict volcanic arcs in the Middle Jurassic: implication for the formation of the Dexing porphyry copper deposit, Southeastern China. Lithos 150, 85–100.
Lu, Y.F., Ma, L.Y., Qu, W.J., Mei, Y.P., Chen, X.Q., 2006. U-Pb and Re–Os isotope geochronology of Baoshan Cu–Mo polymetallic ore deposit in Hunan province. Acta Petrol. Sin. 22, 2483–2492 (in Chinese with English abstract).
Ludwig, K.R., 2003. User's Manual for Isoplot 3.0: Geochronological Toolkit for Microsoft Excel. Berkeley Geochronology Center Special Publication, 4, pp. 70.
Ma, Q., Xu, Y.G., Zheng, J.P., Sun, M., Griffin, W.L., Wei, Y., Ma, L., Yu, X.L., 2016. High–Mg adakitic rocks and their complementary cumulates formed by crystal fractionation of hydrous mafic magmas in a continental crustal magma chamber. Lithos 260, 211–224.
Mahoney, J.J., Frei, R., Tejada, M.L.G., Mo, X.X., Leat, P.T., Nagler, T.P., 1998. Tracing the Indian Ocean mantle domain through time: isotopic results from old west Indian, east Tethyan, and South Pacific seafloor. J. Petrol. 39, 1285–1306.
Mao, J.W., Cheng, Y.B., ChEn, M.H., Pirajno, F., 2013. Major types and time–space distribution of Mesozoic ore deposits in South China and their geodynamic settings. Mineral. Depos. 48, 267–294.
Mao, J.W., Xie, G.Q., Li, X.F., Zhang, C.Q., Mei, Y.X., 2004. Mesozoic large scale mineralization and multiple lithospheric extension in South China. Earth Sci. Front. 11, 45–55 (in Chinese with English abstract).
Mao, W., Zhong, H., Zhu, W.G., Liu, X.G., Zhao, X.Y., 2018. Magmatic–hydrothermal evolution of the Yuanzhuding porphyry Cu–Mo deposit, South China: insights from mica and quartz geochemistry. Ore Geol. Rev. 101, 765–784.
Maury, R., Calmus, T., Pallares, C., Benoit, M., Grégoire, M., Aguillón-Robles, A., Bellon, H., Bohn, M., 2009. Origin of the adakite–high–Nb basalt association and its implications for postsubduction magmatism in Baja California. Mexico: discussion. Geol. Soc. Am. Bull. 121, 1465–1469.
McCulloch, M.T., Gamble, J.A., 1991. Geochemical and geodynamical constraints on subduction zone magmatism. Earth Planet. Sci. Lett. 102, 358–374.
Mi, J.R., Yuan, S.D., Xuan, Y.S., Zhang, D.L., 2018. Zircon U-Pb ages, Hf isotope and trace element characteristics of the granodiorite porphyry from the Baoshan-Dafang ore district, Hunan: implications for regional metallogeny. Acta Petrol. Sin. 34 (9), 2548–2564 (in Chinese with English abstract).
Moyen, J.F., Laurent, O., Chelle-Michou, C., Couzinié, S., Vanderhaeghe, O., Zeh, A., Villaros, A., Gardien, V., 2017. Collision vs. subduction–related magmatism: two contrasting ways of granite formation and implications for crustal growth. Lithos 277, 154–177.
Moyen, J.F., Martin, H., 2012. Forty years of TTG research. Lithos 148, 312–336.
Mungall, J.E., 2002. Roasting the mantle: slab melting and the genesis of major Au and Aurich Cu deposits. Geology 30, 915–918.
Nandedkar, R., Ulmer, P., Müntener, O., 2014. Fractional crystallization of primitive, hydrous arc magmas: an experimental study at 0.7 GPa. Contrib. Mineral. Petrol. 167, 1–27.
Oyarzun, R., Marquez, A., Lillo, J., Lopez, I., Rivera, S., 2002. Reply to discussion on "Giant versus small porphyry copper deposits of Cenozoic age in northern Chile: adakitic versus normal calc–alkaline magmatism" by Oyarzun R, Marquez A, Lillo J, Lopez I, Rivera S (Mineralium Deposita 36: 794–798, 2001). Mineral. Depos. 37,

795–799.
Pettke, T., Oberli, F., Heinrich, C.A., 2010. The magma and metal source of giant porphyrytype ore deposits, based on lead isotope microanalysis of individual fluid inclusions. Earth Planet. Sci. Lett. 296, 267–277.
Plank, T., 2005. Constraints from thorium/lanthanum on sediment recycling at subduction zones and the evolution of the continents. J. Petrol. 46, 921–944.
Plank, T., Langmuir, C.H., 1998. The geochemical composition of subducting sediment and its consequences for the crust and mantle. Chem. Geol. 145, 325–344.
Polat, A., Kerrich, R., 2001. Magnesian andesites, Nb–enriched basalts–andesites, and adakites from late Archean 2.7 Ga Wawa greenstone belts, Superior Province, Canada: implications for late Archean subduction zone petrogenetic processes. Contrib. Mineral. Petrol. 141, 36–52.
Ren, L., Bao, Z.W., Zhang, J., Li, K.X., Huang, W.T., Luo, Z.B., Liang, H.Y., 2019. Magmatic response to slab tearing and resultant crustal evolution during scissor-like oblique continental collision: Insights from Triassic mafic and felsic intrusions in the Qinling orogen, China. Lithos 344–345, 68–85.
Ren, L., Liang, H.Y., Bao, Z.W., Zhang, J., Li, K.X., Huang, W.T., 2018. Genesis of the high Sr/Y rocks in Qinling orogenic belt, central China. Lithos 314–315, 337–349.
Richards, J.P., 2003. Tectono–magmatic precursors for porphyry Cu–(Mo–Au) deposit formation. Econ. Geol. 98, 1515–1533.
Richards, J.P., 2009. Postsubduction porphyry Cu–Au and epithermal Au deposits: products of remelting of subduction–modified lithosphere. Geology 37, 247–250.
Richards, J.P., 2013. Giant ore deposits formed by optimal alignments and combinations of geological processes. Nat. Geosci. 6, 911–916.
Richards, J.P., Kerrich, R., 2007. Special paper: adakite-like rocks: their diverse origins and questionable role in metallogenesis. Econ. Geol. 102, 537–576.
Rollinson, H., 1993. In: Using Geochemical Data: Evaluation, Presentation, Interpretation. Longman Singapore Publishers (Pte) Ltd, Singapore, pp. 1–352.
Sajona, F.G., Maury, R.C., 1998. Association of adakites with gold and copper mineralization in the Philippines. C. R. Acad. Sci. Ser. IIA Earth Planet. Sci. 326, 27–34.
Sajona, F.G., Maury, R., Bellon, H., Cotten, J., Defant, M.J., 1996. High field strength element enrichment of Pliocene-Pleistocene island arc basalts, Zamboanga Peninsula, western Mindanao (Philippines). J. Petrol. 37, 693–726.
Silitoe, R.H., 2010. Porphyry copper system. Econ. Geol. 105, 3–41.
Simon, A.C., Pettke, T., Candela, P.A., Piccoli, P.M., Heinrich, C.A., 2006. Copper partitioning in a melt–vapor–brine–magnetite–pyrrhotite assemblage. Geochim. Cosmochim. Acta 70, 5583–5600.
Smoliar, M.I., Walker, R.J., Morgan, J.W., 1996. Re–Os ages of group IIA, IIIA, IVA, and IVB iron meteorites. Science 271, 1099–1102.
Sun, S.S., McDonough, W.F., 1989. Chemical and isotopic systematics of oceanic basalts: implications for mantle composition and processed. Magmatism in Ocean Basins: In: Saunders, A.K., Norry, M.J. (Eds.). Geological Society of London Special Publication 42, 313–345.
Sun, W.D., Huang, R.F., Li, H., Hu, Y.B., Zhang, C.C., Sun, S.J., Zhang, L.P., Ding, X., Li, C.Y., Zartman, R.E., Ling, M.X., 2015. Porphyry deposits and oxidized magmas. Ore Geol. Rev. 65, 97–131.
Sun, W.D., Liang, H.Y., Ling, M.X., Zhan, M.Z., Ding, X., Zhang, H., Yang, X.Y., Li, Y.L., Ireland, T.R., Wei, Q.R., Fan, W.M., 2013. The link between reduced porphyry copper deposits and oxidized magmas. Geochim. Cosmochim. Acta 103, 263–275.
Sun, W.D., Ling, M.X., Yang, X.Y., Fan, W.M., Ding, X., Liang, H.Y., 2010. Ridge subduction and porphyry copper gold mineralization: an overview. Sci. China Earth Sci. 40, 127–137 (in Chinese with English abstract).
Sun, X.M., Tang, Q., Sun, W.D., Xu, L., Zhai, W., Liang, J.L., Liang, Y.H., Shen, K., Zhang, Z.M., Zhou, B., Wang, F.Y., 2007. Monazite, iron oxide and barite exsolutions in apatite aggregates from CCSD drillhole eclogites and their geological implications. Geochim. Cosmochim. Acta 71, 2896–2905.
Tatsumi, Y., Nakamura, N., 1986. Composition of aquaeous fluid from serpentinite in the subducted lithosphere. Geochem. J. 20, 191–196.
Tribuzio, R., Thirlwall, M.F., Vannucci, R., Matthew, F., 2004. Origin of the gabbro–peridotite association from the Northern Apennine Ophiolites (Italy). J. Petrol. 45, 1109–1124.
Tulloch, A.J., Kimbrough, D.L., 2003. Paired plutonic belts in convergent margins and the development of high Sr/Y magmatism: Peninsular Ranges batholith of BajaCalifornia and Median batholith of New Zealand. Geol. Soc. Am. Spec. Paper 374, 1–21.
Wang, G.G., Ni, P., Yao, J., Wang, X.L., Zhao, K.D., Zhu, R.Z., Xu, Y.F., Pan, J.Y., Li, L., Zhang, Y.H., 2015. The link between subduction–modified lithosphere and the giant Dexing porphyry copper deposit, South China: constraints from high–Mg adakitic rocks. Ore Geol. Rev. 67, 109–126.
Wang, G.G., Ni, P., Zhao, K.D., Wang, X.L., Liu, J.Q., Jiang, S.Y., Chen, H., 2012. Petrogenesis of the Middle Jurassic Yinshan volcanic–intrusive complex, SE China: implications for tectonic evolution and Cu–Au mineralization. Lithos 150, 135–154.
Wang, L., Hu, M.G., Yang, Z., Qu, W.J., Xia, J.L., Chen, K.X., 2011. U-Pb and Re–Os geochronology and geodynamic setting of the Dabaoshan polymetallic deposit, northern Guangdong Province, South China. Ore Geol. Rev. 43, 40–49.
Wang, Q., Wyman, D.A., Xu, J.F., Dong, Y.H., Vasconcelos, P.M., Pearson, N., Wan, Y.S., Dong, H., Li, C.F., Yu, Y.S., Zhu, T.X., Feng, X.T., Zhang, Q.Y., Zi, F., Chu, Z.Y., 2008a. Eocene melting of subducting continental crust and early uplifting of central Tibet: Evidence from central–western Qiangtang high–K calc–alkaline andesites, dacites and rhyolites. Earth Planet. Sci. Lett. 272, 158–171.
Wang, Q., Xu, J.F., Jian, P., Bao, Z.W., Zhao, Z.H., Li, C.F., Xiong, X.L., Ma, J.L., 2006. Petrogenesis of adakitic porphyries in an extensional tectonic setting, Dexing, South China: implications for the genesis of porphyry Copper mineralization. J. Petrol. 47, 119–144.
Wang, Y.J., Fan, W.M., Cawood, P.A., Li, S.Z., 2008b. Sr–Nd–Pb isotopic constraints on multiple mantle domains for Mesozoic mafic rocks beneath the South China Block hinterland. Lithos 106, 297–308.
Wang, Y.J., Fan, W.M., Guo, F., Peng, T.P., Li, C.W., 2003. Geochemistry of Mesozoic Mafic Rocks Adjacent to the Chenzhou-Linwu fault, South China: Implications for the Lithospheric Boundary between the Yangtze and Cathaysia Blocks. Int. Geol. Rev. 45, 263–286.
Wilkinson, J.J., 2013. Triggers for the formation of porphyry ore deposits in magmatic arcs. Nat. Geosci. 6, 917–925.
Winchester, J.A., Floyd, P.A., 1977. Geochemical discrimination of different magma series and their differentiation products using immobile elements. Chem. Geol. 20, 325–343.
Xie, Y.C., Lu, J.J., Ma, D.S., Zhang, R.Q., Gao, J.F., Yao, Y., 2013. Origin of granodiorite porphyry and mafic microgranular enclave in the Baoshan Pb–Zn polymetallic deposit, southern Hunan Province: Zircon U-Pb chronological, geochemical and Sr–Nd–Hf isotopic constraints. Acta Petrol. Sin. 29, 4186–4214 (in Chinese with English abstract).
Xu, J.F., Castillo, P.R., 2004. Geochemical and Nd–Pb isotopic characteristics of the Tethyan asthenosphere: implications for the origin of the Indian Ocean mantle domain. Tectonophysics 393, 9–27.
Xu, J.F., Castillo, P.R., Chen, F.R., Niu, H.C., Yu, X.Y., Zhen, Z.P., 2003. Geochemistry of late Paleozoic mafic igneous rocks from the Kuerti area, Xinjiang, northwest China: implications for backarc mantle evolution. Chem. Geol. 193, 137–154.
Xu, X.S., O'Reilly, S.Y., Griffin, W.L., Wang, X.L., Pearson, N.J., He, Z.Y., 2007. The crust of Cathaysia: Age, assembly and reworking of two terranes. Precamb. Res. 158, 51–78.
Zajacz, Z., Candela, P.A., Piccoli, P.M., Wälle, M., Valle-Sanchez, C., 2012. Gold and copper in volatile saturated mafic to intermediate magmas: Solubilities, partitioning, and implications for ore deposit formation. Geochim. Cosmochim. Acta 91, 140–159.
Zhang, B.R., Gao, S., Zhang, H.F., Han, Y.W., 2002. In: Geochemistry of the Qinling Orogenic Belt. Science Press, Beijing, pp. 1–187 (in Chinese).
Zhang, C.C., Sun, W.D., Wang, J.T., Zhang, L.P., Sun, S.J., Wu, K., 2017. Oxygen fugacity and porphyry mineralization: a zircon perspective of Dexing porphyry Cu deposit, China. Geochim. Cosmochim. Acta 206, 343–363.
Zhang, H., Ling, M.X., Liu, Y.L., Tu, X.L., Wang, F.Y., Li, C.Y., Liang, H.Y., Yang, X.Y., Arndt, N.T., Sun, W.D., 2013. High Oxygen Fugacity and Slab Melting Linked to Cu Mineralization: Evidence from Dexing Porphyry Copper Deposits, Southeastern China. J. Geol. 121, 289–305.
Zhang, L., Ren, Z.Y., Nichols, A.R.L., Zhang, Y.H., Zhang, Y., Qian, S.P., Liu, J.Q., 2014. Lead isotope analysis of melt inclusions by LA–MC–ICP–MS. J. Anal. At. Spectrom. 29, 1393–1405.
Zhang, L., Ren, Z.Y., Xia, X.P., Li, J., Zhang, Z.F., 2015. IsotopeMaker: a Matlab program for isotopic data reduction. Int. J. Mass Spectrom. 392, 118–124.
Zhao, G.C., Cawood, P.A., 2012. Precambrian geology of China. Precamb. Res. 222–223, 13–54.
Zhao, G.C., Wang, Y.J., Huang, B.C., Dong, Y.P., Li, S.Z., Zhang, G.W., Yu, S., 2018. Geological reconstructions of the East Asian blocks: from the breakup of Rodinia to the assembly of Pangea. Earth Sci. Rev. 186, 262–286.
Zhao, L., Zhou, X., Zhai, M., Santosh, M., Ma, X., Shan, H., Cui, X., 2014. Paleoproterozoic tectonic transition from collision to extension in the eastern Cathaysia Block, South China: evidence from geochemistry, zircon U-Pb geochronology and Nd–Hf isotopes of a granite–charnockite suite in southwestern Zhejiang. Lithos 184–187, 259–280.
Zhong, J., Chen, Y.J., Pirajno, F., 2016. Geology, geochemistry and tectonic settings of the molybdenum deposits in South China: a review. Ore Geol. Rev. 81, 829–855.
Zhong, L.F., Li, J., Peng, T.P., Xia, B., Liu, L.W., 2013. Zircon U-Pb geochronology and Sr–Nd–Hf isotopic compositions of the Yuanzhuding granitoid porphyry within the Shi-Hang Zone, South China: petrogenesis and implications for Cu–Mo mineralization. Lithos 177, 402–415.
Zhong, L.F., Xia, B., Liu, L.W., Li, J., Lin, X.G., Xu, L.F., Lin, L.Z., 2010. Metallogenic geochronology of Yuanzhuding Cu–Mo deposit in western Guangdong–eastern Guangxi metallogenic belt and its geological significance. Miner. Depos. 29, 395–404 (in Chinese with English abstract).
Zhou, M.F., Yan, D.P., Kennedy, A.K., Li, Y., Ding, J., 2002. SHRIMP U-Pb zircon geochronological and geochemical evidence for Neoproterozoic arc–magmatism along the western margin of the Yangtze Block, South China. Earth Planet. Sci. Lett. 196, 51–67.
Zou, Y.Q., Chen, X.L., Huang, W.T., Zhang, J., Liang, H.Y., Xu, J.F., Chen, L., 2017. Identification of an Early-Middle Jurassic oxidized magmatic belt, south Gangdese, Tibet, and geological implications. Chin. Sci. Bull. 62, 888–898.